KERNFORSCHUNGSZENTRUM

KARLSRUHE

Dezember 1974 KFK 2061

Institut für Neutronenphysik und Reaktortechnik
Projekt Schneller Brüter

MANDI – A Many-group Diffusion and P_1 Code in One Space Dimension

H.B. Stewart

GESELLSCHAFT
FÜR
KERNFORSCHUNG M.B.H.

KARLSRUHE

GESELLSCHAFT FÜR KERNFORSCHUNG M. B. H.

KARLSRUHE

KERNFORSCHUNGSZENTRUM KARLSRUHE

KFK 2061

Institut für Neutronenphysik und Reaktortechnik

Projekt Schneller Brüter

"MANDI - A Many-group Diffusion and P_1 Code in One Space Dimension"

by

H.B. Stewart

Gesellschaft für Kernforschung mbH., Karlsruhe

Abstract

This report documents the program MANDI, a program for one-dimensional diffusion and P_1 calculations with a large number of energy groups. The code was written following a detailed study of discretization error for such problems, the results of which are reviewed here. Separate sections document the numerical techniques is some detail, and provide basic user's information about program options, input, and evaluated output.

"MANDI - ein Mehrgruppen-Diffusions- und P_1-Code in einer räumlichen Dimension"

Kurzfassung

In diesem Bericht wird das Programm MANDI beschrieben, ein Programm für eindimensionale Mehrgruppen-Diffusions- und P_1-Rechnungen mit vielen Energiegruppen. Nach einer detaillierten Untersuchung der Diskretisierungsfehler für derartige Probleme wurde dieser Code geschrieben. Die Ergebnisse dieser Untersuchung werden im ersten Abschnitt wiedergegeben. Die angewandten numerischen Verfahren werden im zweiten Abschnitt behandelt. Der dritte Teil enthält die nötige Information für die Verwendung des Programms. Hier werden Programmoptions, Eingabe, Ausgabe und Auswertungsmöglichkeiten beschrieben.

Table of Contents

	Page
Introduction	1
Section 1. Discretization Error Analysis	2
Decomposition	4
Mid-region Error	7
Numerical Experiments	9
Rules of Thumb	15
Conclusions	22
Section 2. Numerical Techniques in MANDI	23
P_1 Difference Equations	23
Storage Strategies	28
Neutron Balance Equation	29
Tchebysheff Acceleration	31
Reduction of the P_1 Equations	31
Flowchart	35
Section 3. User's Information	39
Options	39
Input Description	40
Cross Section Data	45
Program Output	48
Program Execution	51
References	53
Appendix A: Sample Problem Description	54
Appendix B: Sample Problem Output	56

Introduction

The goal of the work described in this report was to design and program a computer code to solve efficiently one-dimensional multigroup problems in diffusion and P_1 approximation for fine energy resolution (200-300 energy groups). With such a large number of groups, using the usual fission source iteration scheme for down-scattering only one sees that if the lower triangular scattering matrix is relatively full, most computation time will be spent just adding the scattering contributions into lower energy groups. Since this part of computation time depends only on the scattering matrix and the number of space-energy points, there seem to be two possibilities for better efficiency: (1) special handling of the scattering matrix, and (2) reducing the number of space points to a minimum. The first possibility has already been considered at Karlsruhe, in so far as group cross sections can be generated with a recursive treatment for elastic hydrogen scattering.

The second possibility requires understanding of the discretization error for a particular mesh, in order to choose the mesh with the fewest space points, spaced judiciously to give the desired accuracy. The error analysis, described in Section 1 for the volume-integrated difference equations, was a major part of this work. (Other difference equations had previously been investigated empirically; see Stewart / 7 /. Finite element methods - cf. Strang and Fix / 9 /, Hennart / 5 / - would be another possibility.) Although not all ambitions could be realized, it is hoped that this discretization error analysis will help in choosing efficient spatial meshes for the one-dimensional code MANDI described in Sections 2 and 3, and might point to some understanding of the more complicated multidimensional problems as well.

Zum Druck eingereicht am: 26.3.1975

Section 1. Discretization Error Analysis

We shall look closely at the discretization error, that is, the error due to replacing differential equations of multigroup neutron diffusion by finite difference equations on a given spatial mesh. Analyzing specifically the diffusion approximation, we begin by considering the simple case of a single equation with a given source; this simple case is the basic element of the usual fission source iterations with down-scattering only. We derive a general expression for this single-equation error.

In slab geometry, the diffusion equation is simply

$$-D\phi''(x) + \sigma\phi(x) = s(x) \tag{1}$$

which holds on each subinterval (a_i, a_{i+1}) of an interval $[a_o, a_I]$; we suppose that D and σ are constant on each subinterval. Across each interface point a_i, $0 < i < I$, the flux $\phi(x)$ and the current $J(x) = -D\phi'(x)$ shall be continuous, and a boundary condition of the type $J + \alpha\phi = 0$ will be imposed at a_o and at a_I. The more general equation

$$r^{1-n}((d/dr)r^{n-1}(-D\, d\phi/dr)) + \sigma\phi = s \tag{2}$$

holds in three geometries: $n=1$ for slab, $n=2$ for cylinder, and $n=3$ for sphere.

Let a mesh be given with mesh interval endpoints r_k and midpoints $r_{k+1/2}$. A common difference scheme

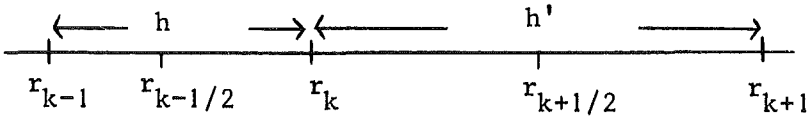

for these equations is derived by integrating the differential equation over volume from $r_{k-1/2}$ to $r_{k+1/2}$, then making simple approximations of $\int \sigma\phi\, dV$, $\int s\, dV$, and $d\phi/dr$ (cf. Section 2).

The resulting edge-centered volume-integrated difference formulas

$$r_{k-1/2}^{n-1} D(\phi_k - \phi_{k-1})/h - r_{k+1/2}^{n-1} D(\phi_{k+1} - \phi_k)/h'$$

$$+ \frac{1}{n} (r_{k+1/2}^{n} - r_{k-1/2}^{n})(\sigma\phi_k - s_k) = 0 \qquad (3)$$

(here for continuous D, σ, and s) form a system of three-point difference equations which, together with the two boundary conditions, can be solved by Gaussian elimination.

Since the difference equations were derived approximately, their exact solution will deviate from the values of the exact solution of (2) by some amount which we call the discretization error. The error depends on the approximations used in deriving (3) and on the particular mesh used.

In approximating the removal and source terms of (2), $\sigma\phi$ and s, we used e.g.

$$\int_{k-1/2}^{k+1/2} s(r)\, r^{n-1}\, dr \simeq s(r_k) \int_{k-1/2}^{k+1/2} r^{n-1}\, dr \qquad (4)$$

To find the error in this approximation we assume that $s(r)$ is smooth near r_k and expand s in a Taylor series about r_k. We give the results for equidistant mesh spacing, i.e. $h=h'$. If we also remember to expand r^{n-1} about r_k, the error in (4) becomes

$$(h^3/24)\, r_k^{n-1}\, (s^{(2)} + 2(n-1)/r_k \cdot s^{(1)}) + O(h^4) \quad ,$$

where $s^{(i)}$ is the i-th derivative of s at r_k. A similar error results from approximating the integral of $\sigma\phi$. The derivative term in (2) is an exact derivative for volume integration, so the integral is not an approximation; but $d\phi/dr$ at $x=r_{k\pm1/2}$ is approximated, by a finite difference. Since ϕ is smooth if s and the coefficients are, we expand ϕ in a Taylor series and find an error contribution

$$(h^3/24)\ Dr_k^{n-1}\ (\phi^{(4)} + (n-1)/r_k \cdot \phi^{(3)}) + O(h^4).$$

Setting all terms together we find that the error =

$$(h^3/24)\ r_k^{n-1}\Big\{ D(\phi^{(4)} - (n-1)/r_k \cdot \phi^{(3)}) + (\sigma\phi^{(2)} - s^{(2)}) + 2(n-1)/r_k \cdot (\sigma\phi^{(1)} - s^{(1)}) \Big\} + O(h^4). \tag{5}$$

Note that this is not the error in ϕ but the error in the difference equation, i.e. the amount which must be added to the difference equation (3) in order that (3) be satisfied by the exact solution ϕ of the differential equation (2). In the case of slab geometry, $n=1$, this simply is

$$\text{error} = (h^3/24)\{D\phi^{(4)} - \sigma\phi^{(2)} - s^{(2)}\} + O(h^4) \tag{6}$$

Decomposition into Slowly Varying Part and Interface Contribution

The error expression (5) is exact in all cases where the mesh spacing is equidistant. (If $h=h'$, an error term of order h^2 appears, where h is the larger interval width.) The disadvantage of (5) is that it involves the unknown exact solution ϕ of the differential equation (2), and in fact derivatives of ϕ up to fourth order. To ameliorate this difficulty, as well as to reach a better understanding of the discretization error in realistic heterogeneous problems, we introduce the decomposition below.

We continue to suppose that D,σ, and h are constant on each subinterval (a_i, a_{i+1}) and that $s(r)$ is smooth on each subinterval. Considering slab geometry first, we expand $s(r)$ on (a_i, a_{i+1}) in a Taylor series about the origin $r=0$:

$$s_i = \sum_j s_j^i\ r^i/j!$$

Now on the interval (a_i, a_{i+1}) we shall seek to represent the exact solution ϕ of differential equation (1) in two parts: a particular solution of the inhomogeneous D.E., plus terms near the subinterval endpoints which fit the continuity conditions and are solutions of the homogeneous equation. For subinterval i,

$$\phi_i = \psi_i + c_i^{\ell} h_i^{\ell} (r-a_i) + c_i^{r} h_i^{r} (a_{i+1}-r) \qquad (7)$$

where ψ_i is the particular solution of the differential equation (1), and h_i^{ℓ}, h_i^{r} are the two linearly independent solutions of the homogeneous differential equation on subinterval i. We imagine h_i^{ℓ} fitting continuity (or boundary) conditions at the left end, h_i^{r} at the right end of the subinterval.

For ψ_i we choose the particular solution gotten in the following way. Let ψ_i have a Taylor series

$$\psi_i = \sum_j \psi_j^i r^j / j!$$

Upon substituting into the differential equation we get the recursion relation

$$-D_i \psi_{j+2}^i + \sigma_i \psi_j^i = s_j^i \quad , \quad j=0,1,2,\ldots$$

If the series for s_i ends in a finite number of terms, then ψ_i is uniquely determined by assuming that it also has a finite number of terms. Or we may assume that the source s_i is slowly varying in the sense that its derivatives $s_i^{(k)}$ satisfy

$$s_i \;>>\; L^2 s_i^{(2)} \;>>\; L^4 s_i^{(4)} \;>>\; \ldots$$

$$Ls_i^{(1)} \;>>\; L^3 s_i^{(3)} \;>>\; L^5 s_i^{(5)} \;>>\; \ldots \quad ,$$

i.e. s_i varies slowly on the scale of diffusion lengths $L = (D/\sigma)^{1/2}$; then there is a unique convergent series for ψ_i, and in this case we would find that $\psi^i_j \simeq s^i_j/\sigma$, or $\psi_i \simeq s_i/\sigma$.

Two solutions of the homogeneous differential equation in slab geometry are $\exp(\pm r/L)$, so that for example we might take $h^\ell_i = \exp((a_i - r)/L_i)$. Once a particular solution ψ_i has been chosen on each subinterval, the continuity and boundary conditions supply a set of 2I linear equations which uniquely determine the coefficients c^ℓ_i, c^r_i. In this way we can decompose ϕ_i according to (7). Notice that if a subinterval is several diffusion lengths wide, $a_{i+1} - a_i >> L_i$, then $\exp((a_{i+1} - a_i)/L_i) \simeq 0$. This means that if a subinterval is several diffusion lengths wide, h^ℓ_i equals one at the left and nearly vanishes at the right end of the subinterval, while the converse holds for h^r_i. In this case h^ℓ_i would clearly be associated with the continuity conditions at the left interface, and h^r_i with the right interface.

In deriving this decomposition we have chosen slab geometry for convenience. The same steps can be repeated for cylinder and sphere geometries. In general, two solutions of the homogeneous equation are, in the notation of / 1 /,

$$r^{(1-n)/2} H^{(1)}_{(1-n)/2}(ir/L), \quad r^{(1-n)/2} H^{(2)}_{(1-n)/2}(ir/L)$$

involving Hankel functions (cf. Courant and Hilbert / 3 /, p.244). The expressions reduce to $\exp(\pm r/L)$ for $n=1$ and to $(1/r)\exp(r/L)$ for $n=3$; for $n=2$ the Bessel functions cannot be eliminated. In case $n>1$, a Taylor series for s and ψ is not convenient in the above derivation, and one does better to use a power series corresponding in form to the expansion of the appropriate Bessel functions. Thus there are complications, but no change in the ideas.

To repeat, we have both a conceptual and an (approximate) numerical decomposition of the true solution ϕ into particular solutions ψ_i, which we will suppose to be slowly varying, plus special terms of exponential character near the interfaces due to discontinuous D, σ, and s. These latter terms die off exponentially on the scale of diffusion lengths going away from the interface.

Mid-region Error

Both terms above - the slowly varying particular solution and the fitting terms for interfaces - will contribute to the discretization error as in expressions (5) or (6). Although the pointwise error corresponding to the fitting terms may be large near the interfaces, its importance is limited in space due to the exponential decay (of the error as well as the term itself). For wide subintervals, the slowly varying particular solution may contribute strongly to the volume integral of error. The relative importance of the two parts will be discussed more specifically below; at the moment we emphasize that the slowly varying part is probably more important to volume integral error. We give a simplification of error formula (5) with this in mind, followed by tests on realistic numerical examples.

The goal of the experiments was to reconstruct approximately the discretization errors in each group of a multigroup eigenvalue problem and estimate the net effect on the eigenvalue k_{eff}. Thus the volume integral of error in mid-region for each subinterval (zone) was of interest. To find this from (5), we first note that

$$\phi^{(2)} + (n-1)/r \cdot \phi^{(1)} = r^{1-n} \frac{d}{dr} r^{n-1} \frac{d}{dr} \phi$$

$$= \nabla \cdot \nabla\phi.$$

Also

$$D\phi^{(4)} + D(n-1)/r \, \phi^{(3)} = \nabla \cdot D\nabla(\phi^{(2)})$$

$$= \frac{d^2}{dr^2} (\nabla \cdot D\nabla\phi) + \frac{n-1}{r^2} D\phi^{(2)} + \frac{2(n-1)}{r^3} D\phi^{(1)}$$

If $n=1$, the last two terms vanish. If $n>1$, they may be negligible at least for $r>>1$; this will be tested in numerical examples. If we do choose to drop those terms, we can apply the original differential equation to the first term and get

$$\frac{d^2}{dr^2}(\nabla \cdot D\nabla\phi) = \frac{d^2}{dr^2}(\sigma\phi - s)$$

and simplify (5) to

$$(h^3/12)r^{n-1}\{(\sigma\phi^{(2)} - s^{(2)}) - (n-1)/r \cdot (\sigma\phi^{(1)} - s^{(1)})\} + O(h^4)$$

which reduces further to

$$\text{error} \simeq (h^3/12)r^{n-1}\{r^{1-n}\frac{d}{dr}r^{n-1}\frac{d}{dr}(\sigma\phi - s)\} + O(h^4) \qquad (8)$$

Again this estimates the amount which would have to be added to the difference equation (5) to make it true for values ϕ of the exact solution of the differential equation (2). To find the resulting error in the solution $\{\phi_k\}$ of the difference equations, we consider solving those difference equations (3), perturbed on the right hand by (8), using Gaussian elimination. Without repeating the details (see e.g. Stewart / 6 /), we claim that in the mid-region of a subinterval with constant diffusion length, error in (8) translates to error in ϕ_k as follows: (a) if $h>L$, Gaussian elimination does not multiply the errors; (b) if h is noticeably smaller than one diffusion length, then (after normalizing the difference equation so that the coefficient of ϕ_{k-1} in the k-th equation is one) Gaussian elimination multiplies the initial perturbation by a factor $(L/h)^2$. In other words, the error in ϕ_k ends up $(L/h)^2$ times larger than the error in the (normalized) difference equations. Applying this to expression (8) with normalization h/Dr^{n-1}, we get

$$\text{error}(\phi) \simeq (h^2/12)(L^2/D)\{r^{1-n}\frac{d}{dr}r^{n-1}\frac{d}{dr}(\sigma\phi - s)\} + O(h^3)$$

for $h<L$, which we can easily integrate over any volume where ϕ and s are smooth to

$$\frac{1}{2(n-1)\pi}\int_{a_i}^{a_{i+1}} \text{error}\ (\phi)\ dV \simeq \int_{a_i}^{a_{i+1}} \frac{h^2}{12}\ \frac{1}{\sigma}\ r^{1-n}\ \frac{d}{dr}\ r^{n-1}\ \frac{d}{dr}(\sigma\phi - s)r^{n-1}\ dr$$

$$\simeq \frac{h^2}{12}\left[r^{n-1}\ \frac{d}{dr}\ (\phi - s/\sigma)\right]_{r=a_i}^{r=a_{i+1}} + O(h^3) \qquad (9)$$

This gives an easy approximate formula for the volume integral of error. It involves only certain differences of first derivatives of ϕ and s, rather than the derivatives up to fourth order in (5). Thus there is some hope that (9) could be employed to estimate discretization error for difference equation (3) without catastrophic numerical instability.

Numerical Experiments

In order to test the ideas above, and to investigate the feasibility of error estimation for multigroup diffusion problems, a number of simple but realistic sample problems were run with an experimental version of MANDI. The code was modified to produce estimates for the discretization error in k_{eff}. This requires, in addition to the one-group, fixed-source estimates above, a method of handling the multigroup structure, which we now describe.

In outline the multigroup error estimation follows the same path as the multigroup flux calculation which is governed by the equations

$$-\nabla \cdot D_g \nabla\phi_g + \sigma_g^{rem}\phi_g = \sum_{g'<g} \sigma_{g'\to g}^{scat}\ \phi_{g'} \qquad (10)$$

$$+ \frac{1}{k_{eff}}\ \chi_g \sum_{g'} \nu\ \sigma_{g'}^{fis}\ \phi_{g'}\ ,\ g=1,\ldots G.$$

Errors incurred in one group will be distributed to other groups via scattering and fission, just as the flux in one group gives rise to flux in other groups. As a first approximation we consider only the the transfer of error via scattering, not fission; this corresponds to

the assumption that scattering is more frequent than fission, which often holds where diffusion theory applies. Following this assumption we ignore error arising in the fission source term of (10), and concentrate on the propagation of errors from higher to lower energy groups via the scattering source term; again the measure of this assumption will be in the sample problems. In any group g the discretization error will then have two parts: (I) the error in discretizing the group g equation, which would occur if the scattering source were exact; (II) the error which is an imprint on ϕ_g of the error in the scattering source for group g - this latter being due to the error in discretizing groups $g'<g$, it would occur even if there were no error in discretizing group g. Numerical examples showed that type II error is substantial, and essential to multigroup error estimating: a method which did not trace propagation of error from group to group, at least via scattering, would grossly underestimate errors in multigroup problems.

For each power iteration, the multigroup error estimating routine does the following in the case of down-scattering only: After the flux in group 1 is found this ϕ_1 and the net source s_1 in group 1 are substituted in place of the exact ϕ_1 and s_1 in the error estimate (9), which involves the first derivatives of ϕ_1 and s_1 near the ends of each zone. Actually we stay one or two diffusion lengths away from interfaces to avoid the fitting terms in (7) and concentrate on the slowly varying part of ϕ_1 in each zone. Applying (9) in this way estimates the volume integral error of type I for group 1. Since this is the group of highest energy, there is no inscattering, and ignoring error from the fission source there is no type II error in group 1. For groups of lower energy, type I error is found in the same way as for group 1. In addition, error in the scattering source is now to be considered. For group g, the total errors (types I and II) for groups of higher energy ($g'=1,2,\ldots g-1$) multiplied by the scattering cross sections into g give the error in the scattering source. We now assume as a first approximation that this translates into flux error simply through multiplication by $1/\sigma_g^{rem}$. This is the type II error for group g.

In this way discretization error is estimated for each group. Multiplied by $\nu\sigma^{fis}$ and summed, these group errors yield the approximate error in the new fission source guess, again volume integrated for each zone. This leads to an error estimate for k_{eff}.

This scheme for estimating zone-wise volume integral discretization error, and error in k_{eff}, was tested with some simple but realistic 26-group fast reactor problems. These are models of the ZPR-III-10 fast assembly, already used for test problems as described in Kiefhaber /10/, Stewart /7/. Both a one-zone (bare homogeneous core) and a two-zone (core and blanket) 26-group structure were investigated in slab and spherical geometry.

The homogeneous 26-group problems provide the simplest test of the scheme described above. In slab geometry a mesh of 34 steps was chosen, representing about five steps per diffusion length. An error estimate was given after each outer iteration. The discretization error for this problem is known exactly by comparison with an equivalent zero-dimensional calculation, which is verified by a 1-D calculation with much finer mesh. The true error and the error estimates for k_{eff} are:

One Zone, Slab Geometry

true discretization error in k_{eff}	.0062 %k
final estimate	.0087 %k
estimate after third iteration	.0084 %k

These estimates, while not razor-sharp, are reasonably good, and could certainly be helpful. They suggest that the multigroup estimating scheme is not in principle wrong. If similar estimates were possible for more complicated problems, the method would indeed be useful.

The one-zone problem was also calculated in spherical geometry, giving the following results:

One Zone, Sphere Geometry

true discretization error in k_{eff}	.028 %k
final estimate	.040 %k
estimate after third iteration	.040 %k

Note that in both cases the estimate after three iterations was essentially as good as the final estimate.

Naturally the homogeneous problem is an easy one to estimate, for even in multigroup form the errors in each group are non-negative at all space points, and have the same spatial distribution as the flux (which is the same for all groups). A heterogeneous problem will necessarily be more complicated. Because of the heterogeneities, flux shapes in some groups will have inflections; recalling from (8) that the discretization error depends on the second derivative, i.e. the curvature, of the flux and of the group source, we see that the error in one group may have different signs at different locations. In fact this could even happen in a group with no inflection, as the flux shape and source shape could still be quite different. Furthermore, due to shape variations from group to group, it could be that at a given location the error is positive in some groups and negative in others. Examples of group flux shapes taken from the two-zone test problem are given in Figure 1.

For this heterogeneous test problem with core and blanket no exact solution was available; thus the true discretization error was found by comparison with results for a much finer mesh (also checked with a separate program using the same difference formulas). With 23 mesh steps in core and 33 in blanket (about 3 steps per diffusion length), the results of estimation were:

Two Zones, Slab Geometry

true discretization error in k_{eff}	-.0033 %k
final estimate	+.0043 %k
estimate after third iteration	+.0042 %k

Regarding for a moment the true error, we note it is smaller in magnitude than for the one-zone case, even though that previous mesh was finer (in steps per diffusion length). Furthermore, the sign of the true error has reversed. These facts confirm that compensation

Figure 1: Some Group Flux Shapes from 26-group 2-zone Test Problem

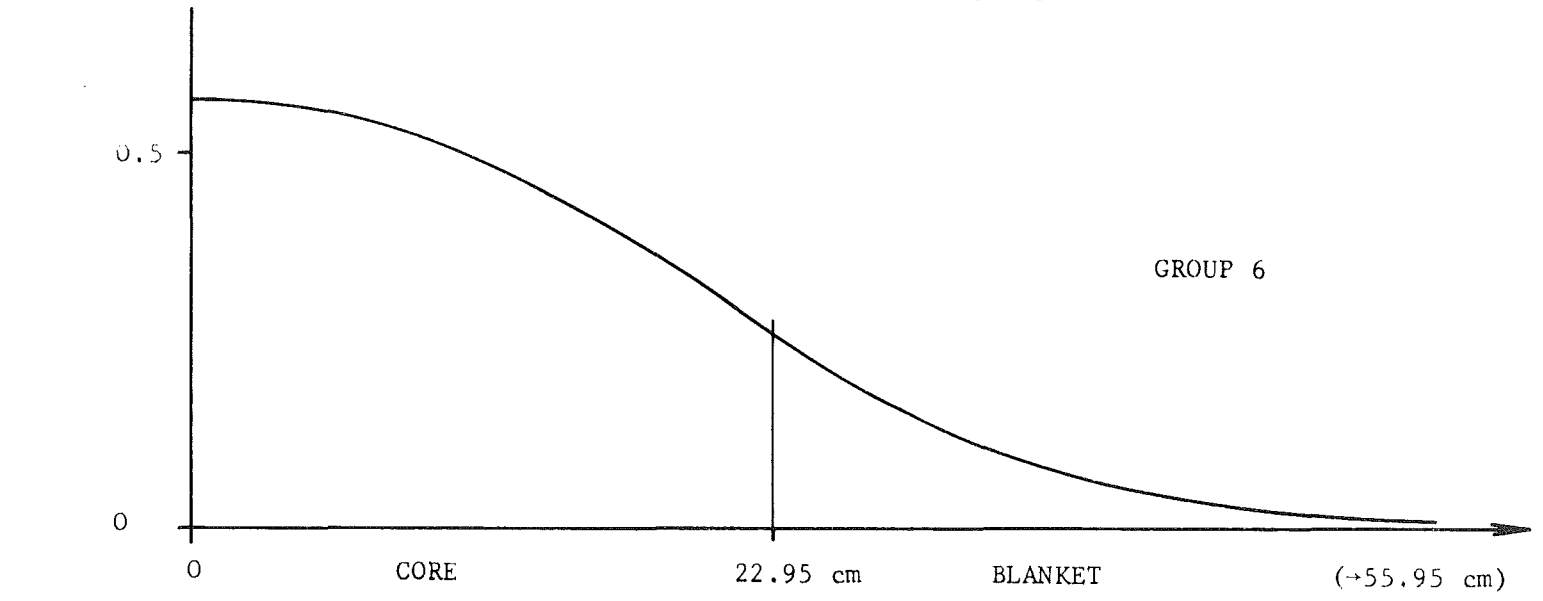

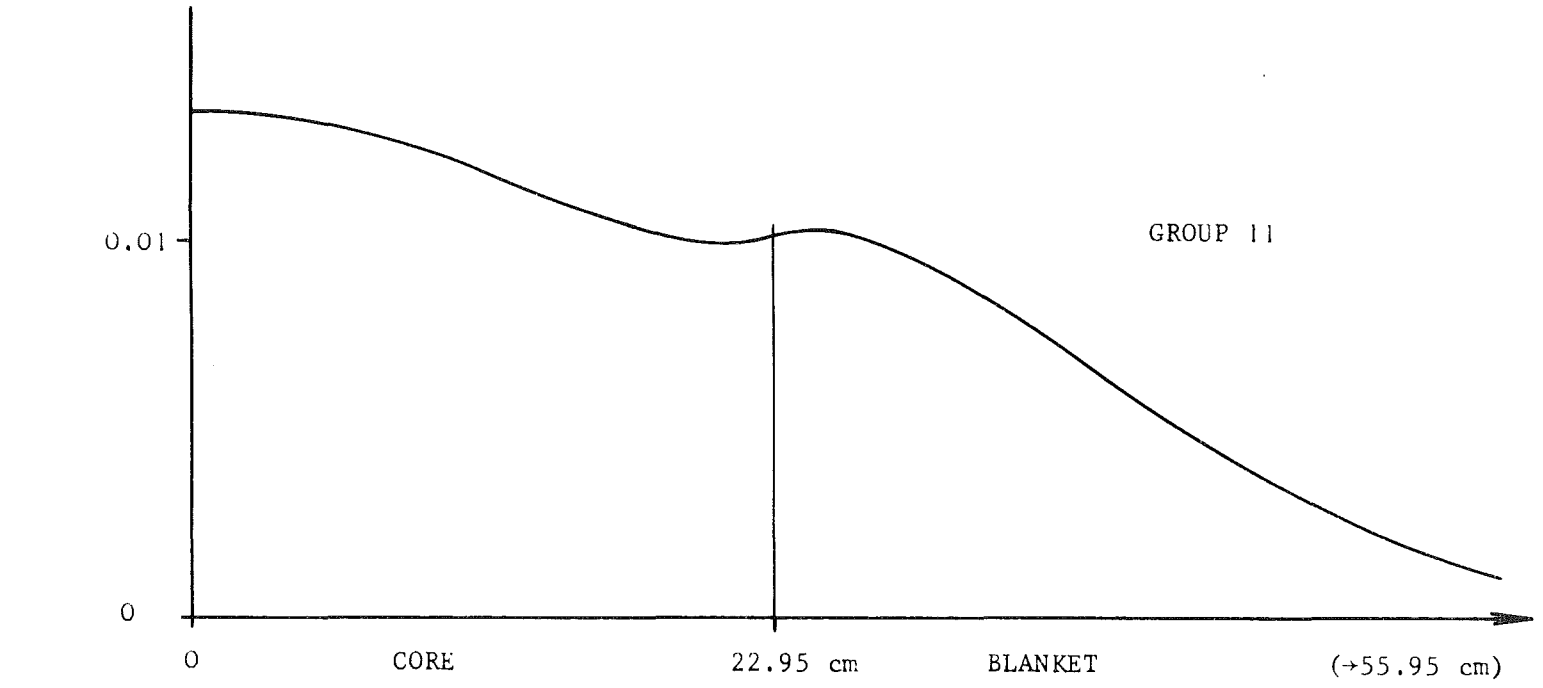

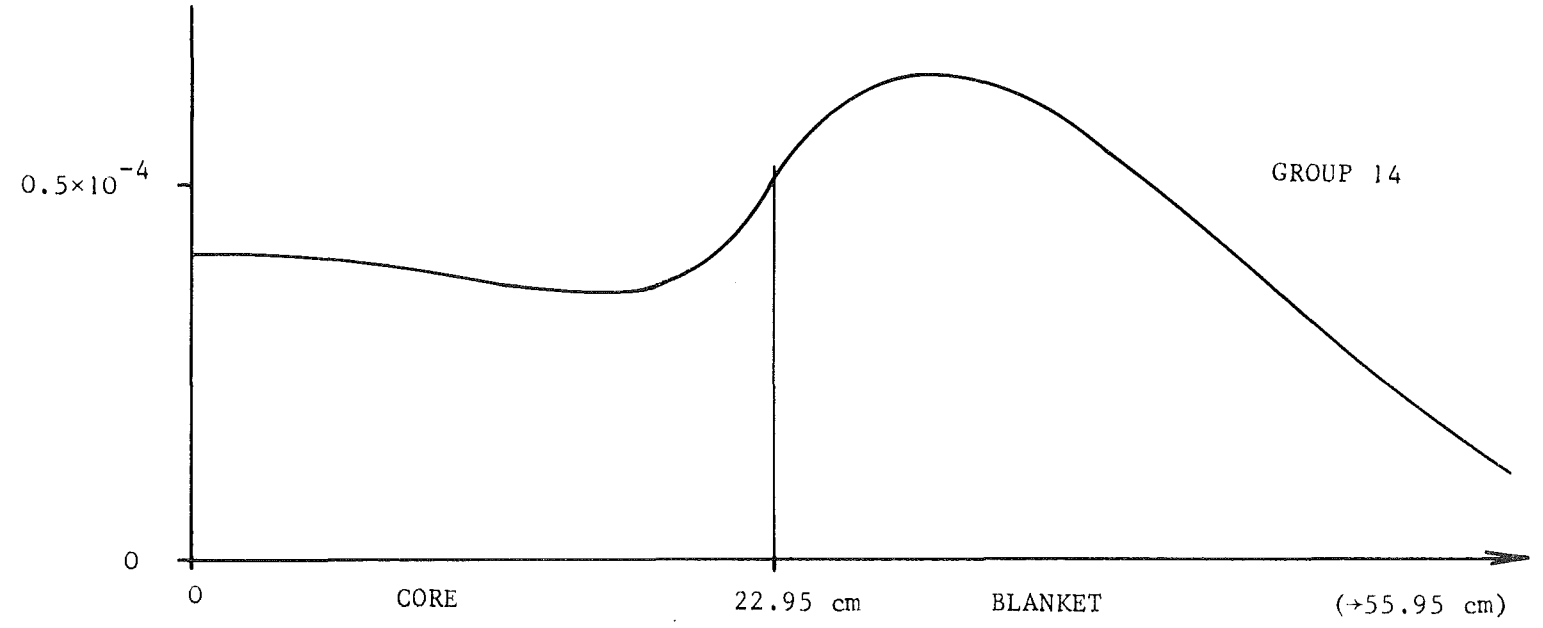

of negative and positive errors is an important feature of this problem.

As for the error estimate, we see that it has roughly the right magnitude but the wrong sign. A careful check of the error estimating subroutine showed that it should always deliver the proper sign; indeed it did for the one-zone problems. The only possible conclusion is that the error estimate for this two-zone problem is seriously wrong, and the apparent agreement for the absolute value of the estimate is an accident. This view is confirmed by results of the corresponding sphere problem:

Two Zones, Sphere Geometry

true discretization error in k_{eff}	-.0066 %k
error estimate	+.023 %k
estimate after third iteration	+.021 %k

A careful review of the error estimation showed that the situation in these failed cases is complicated. In most of the groups which contribute heavily to the error in k_{eff}, the flux profile looks roughly like the upper curve in Figure 1. Curvature in zone 1 (core) is negative, while in zone 2 (blanket) the curvature is positive. The same holds for the scattering source profiles in these groups. The curvatures of ϕ and s/σ are comparable in magnitude, so the sign of expression (9) for the approximate error will depend on which curvature is larger. In both zones, the difference of the two curvatures turns out to be negative in some groups and positive in others. In the one-zone problem this did not occur; even the difference of curvatures had the same sign in all groups. For the two-zone problem, one can only say that compensation of negative and positive errors is substantial, so that our estimates of the errors in each group no longer combine to give an accurate estimate of the whole.

Although the two-zone 26-group problem is numerically too complicated for our error analysis to yield a useful estimate, the problem itself is not complicated by the standards of typical one-dimensional diffusion

calculations. Thus the above scheme must be considered as a failure in terms of practical quantitative analysis. However, some understanding of discretization error for 1-D multigroup problems has been gained. We shall now try to crystallize some that understanding for qualitative use.

Dealing with Discretization Error - Rules of Thumb

Let us return to the decomposition (7). Equation (7) tells us that the exact solution of a single group equation consists in each zone of a particular solution plus fitting terms. In any zone which is wide in terms of diffusion lengths, we assume that the particular solution is slowly varying, and that each of the two fitting terms insures the continuity conditions at one end of the subinterval.

As mentioned before, it seems likely that the exponential terms may cause a relatively large error near the interfaces, but due to decay this contribution will not be felt more than a very few diffusions lengths from the interface. The slowly varying particular solution will be associated with a discretization error which may be small at each point, but which gains importance when summed over a wide region and spread through the multigroup structure. With these ideas in mind, a special form of space mesh has been allowed in the code MANDI.

The mesh used by MANDI must be the same for all energy groups, but may be non-uniform in space. First a uniform division of each zone is given, as is usual in one-dimensional codes; this we call the basic mesh. This basic mesh corresponds to the slowly varying fluxed. Then a refinement option allows any step in the basic mesh to be subdivided into any integral number of refined mesh steps. This refinement is directed at the fitting terms, and is meant for use near the interfaces.

More specifically, refinement is useful for the resonance groups which can be pronounced in the 208-group structure used at Karlsruhe. (This 208-group structure is derived from the ABBN 26-group structure by subdividing each of the 14 highest energy groups in ABBN into 14 subgroups of equal lethargy; the remaining 12 ABBN groups are used intact

giving 14 x 14 + 12 = 208 groups.) In well resolved resonance groups the diffusion length can be much shorter than the average. This need not mean a fine mesh throught the zone, since in mid-zone the flux will still not vary too rapidly. But near an interface, the fitting terms will reflect the short diffusion length and may have sharp variations. Thus for flux in the neighborhood of an interface in a resonance group, mesh refinement may prove indispensable.

Of course such a refinement which is added because of a resonance group should help accuracy in other groups as well. It is difficult to say whether the improvement in one group or the other has more effect on the accuracy of k_{eff}. But certainly, as the following example shows, the local improvement in flux values in groups near resonance can be dramatic. Table 1 shows results of 208-group calculations for the ZPR-III-48 assembly, again a two-zone core-and-blanket model. A zone-wise uniform mesh is compared with a locally refined mesh. The uniform mesh consisted of 60 intervals in core and 40 in blanket. The non-uniform mesh was based on 30 intervals in core, 20 in blanket; refinement up to a factor 8 was added to bring the total number of intervals to 71. (Both cases were compared with a 1000-step mesh which was taken as exact.)

Error Criterion	Uniform (100)	Non-uniform (71)
k_{eff}	.01 %	.01 %
fission source in core	.06 %	.06 %
flux at interface near resonance	2.6 %	0.1 %

Table 1. Uniform vs. Non-uniform mesh comparison.

Obviously the use of refinement was a cheap means of achieving good accuracy for the resonance group flux. One should also notice that the same k_{eff} accuracy was achieved by both meshes, with a 30 % savings for the non-uniform mesh. (The number of mesh steps is nearly proportional to computation time and to core storage requirement.)

A non-uniform mesh can be designed for a given problem in the following manner. First one needs to choose a basic (zone-wise uniform) mesh; a suggestion for this will be given below. Refinements are then added for accuracy in resonance group fluxes, and for improved accuracy in k_{eff}. Refinement can be set at the interfaces so that the most refined mesh step is at least smaller than the diffusion length of the extreme resonance group. If this factor is large (but not much over 10, otherwise the basic mesh is suspect), it should be decreased to one, over a few basic steps moving toward mid-zone. Each pair of neighboring unequal mesh steps causes an $O(h)$ error term, so a large number of gradual changes may be worse than one abrupt one; as a compromise the refinement can be successively halved.

The degree of refinement at a zone end will depend on how strong the resonance is in that zone. For a strong resonance, more refinement is useful. In this case there might also be an abrupt change in step length if the neighboring zone has no resonance and is not refined; some refinement could be added here also, for the sake of a smooth transition.

For a concrete example we explain the refinements used in the 71-point mesh mentioned in Table 1. The core zone has a strong Na resonance, where the diffusion length is only 1/220th of the zone width. Thus a refinement factor of 8 was chosen on the 30-interval basic mesh, so that the smallest refined step, next to the interface, is 1/240th the width of core. The refinement factor of 8 was decreased to 4,2,1 on successive basic mesh steps away from the interface. On the core side of the interface a refinement factor 4 was chosen simply to avoid abruptness; furthermore, the diffusion length in blanket at resonance was about equal to the average, 1/6th of the zone width. Thus the blanket refinement was decreased roughly on the scale of diffusion lengths: 4, 4, 2, 2, 2, 2, 1. The boundary conditions do not usually require refinement, so the final pattern of refinement is:

1 ... 1 2 4 8 // 4 4 2 2 2 2 1 ... 1

Choosing the basic mesh also presents a problem. In fact, if one is only interested in an accurate value of k_{eff}, even in cases where

refinements help noticeably the basic mesh will likely be more important. One trick which may help in this regard, especially with a large number of energy groups, is comparison with an energy-condensed problem. That is, one collapses the problem to a relatively few-group structure, and studies (at relatively low cost) the error behavior of the few-group problem. Apparently, at least in some cases, the effect on k_{eff} of, say, doubling the mesh will be almost the same for the original and for the condensed problem, even if k_{eff} itself changes by condensation. (This may be true only for the three-point volume-integrated difference equations.) To illustrate this, we offer some examples of 208-group calculations and corresponding condensed problems with 26 and fewer groups.

The first series uses the ZPR-III-48 two-zone model mentioned above. Three successive meshes of 25, 50, and 100 basic intervals are compared. Each mesh was refined for the Na resonance. Following a 208-group calculation with the 50 basic interval mesh, the flux integrals and leakages we used to determine rather accurate spectra, and a flux-weighted condensation was performed to the 26-group ABBN structure. The identical meshes we then re-used for 26-group calculations. Table 2 shows the results, namely that the effect of changing to a finer mesh is practically identical in the original and condensed problems.

Of course in this case the value of k_{eff} itself was not much changed by condensation. Further tests were done to see if discretization error also holds the same when k_{eff} changes more noticeably. To this end, new spectra were calculated in the 208-group structure using a coarse mesh (25 basic intervals, no local refinement) and stopping the 208-group calculation after 4 outer iterations (with error in k_{eff} = 1/2 %k). The coarse spectra were used for a new condensation to 26 groups, and to a 5-group structure considered appropriate for ZPR, to a 4-group structure considered inappropriate for ZPR, and finally to one group (each time condensing from 208 groups). The results appear in Table 3, and are quite good, even for the one-group case where k_{eff} itself is somewhat away from the 208-group value.

In a second series of tests, the SUAK assembly UH1B was calculated in a three-zone symmetrized slab model, consisting of a largely uranium core and two reflector plates, the first of iron, the outer of aluminum.

Table 2. Dependence of k_{eff} on Mesh Before and After Condensation
ZPR-III-48 Slab, Accurate Spectra

Basic Mesh Steps	208 groups	26 groups
25	.952875	.953084
50	.953180	.953388
100	.953275	.953482
Δ(50-25)	305	304
Δ(100-50)	95	94

The basic meshes used were: 10, 3, 3 (steps in core, iron plate, aluminum plate); 20, 5, 5; and 40, 10, 10. A refinement factor 2 was used in every basic step adjoining a boundary. Again the spectra for condensation were calculated in 208 groups on a coarse mesh with few (3) outer iterations. It should be mentioned that condensation of the diffusion coefficients was weighted by leakages, and in these leakage spectra the transverse buckling leakages were not included. Table 4 shows the results. Even condensation to 26 groups changed k_{eff} considerably; but in most cases the discretization error behaves as with 208 groups. One exception is the coarse mesh with 26 groups; in this case however the condensation was anomalous, with one of the condensed diffusion coefficients in the steel reflector turning out negative.The one-group condensation is least similar to the original 208-group problem, both in k_{eff} itself and in its error.

Table 3. Dependence of k_{eff} on Mesh Before and After Condensation ZPR-III-48 Sphere, Coarse Spectra

Basic mesh steps	208 groups	26 groups	5 groups	4 groups	1 group
25	.947457	.948043	.947968	.949493	.934919
50	.948409	.948987	.948923	.950430	.935893
100	.948682	.949256	.949194	.950693	.936173
Δ(25-50)	952	944	955	937	974
Δ(100-50)	273	269	271	263	280

Table 4. Dependence of k_{eff} on Mesh Before and After Condensation
SUAK UH1B Symmetrized Slab, Coarse Spectra

Basic Mesh Steps	208 groups	26 groups	4 groups	1 group
16	.907159	.927886	.931124	.939182
30	.907216	.927967	.931190	.939216
60	.907255	.928006	.931222	.939237
Δ(30-16)	57	81	66	34
Δ(60-30)	39	39	42	21

Conclusions

A few highlights of this study of discretization error deserve emphasis.

(1) Theoretically the discretization error in each energy group can be understood as arising from a slowly varying term in each zone, plus terms of given (e.g. exponential) form which relate to interface continuity conditions. The latter errors may be large but only near interfaces; the former may be small at each point but more important when integrated over volume.

(2) The non-uniform mesh, which was included in MANDI with the above decomposition in mind, seems advantageous for heterogeneous many-group problems. Rules of thumb are given for exploiting this advantage. Integral values (i.e. k_{eff}) can be moderately improved with local refinement, and local values may improve dramatically.

(3) In a multigroup problem, errors in one group produce errors in other groups, just as flux influence is propagated. Unfortunately the propagation of error could not be quantitatively reconstructed for heterogeneous problems using the simple approximations studied here.

(4) As a substitute aid to choosing basic mesh, group collapsing seems quite promising. The discretization error in k_{eff} for many-group and for few-group condensed problems often behave nearly the same, even if k_{eff} itself is changed considerably.

On the last point, a further investigation is recommended, including strongly heterogeneous power reactor configurations and multidimensional calculations. Also different collapsing schemes could be tried; the flux and current leakage ($\nabla \cdot J$) weighting mentioned above seemed to work well, but can also especially be risky since current weights can be negative. If further results are as encouraging, a procedure could be envisioned for frequently used multigroup codes which automatically checks discretization error via a condensed problem.

Section 2. Numerical Techniques in MANDI

In this section we attempt to document the more important numerical techniques used in the code MANDI. We include a derivation of the approximate P_1 difference equations, a method of calculating the approximate current J, the utilisation of core storage, explanation of the neutron balance equations, and Tchebysheff acceleration of fission power iterations. We also mention a manipulation of the P_1 equations which in some circumstances could be more efficient than the method used in MANDI; this idea is documented here even though it was not used.

P_1 Difference Equations

Expansion of the angular dependence of the neutron transport equation in spherical harmonics leads to the P_N equations; expansion in the zero-th and first moments only gives the P_1 equations. These involve the total flux $\phi(r)$ and net current $J(r)$ in the radial direction. The multigroup P_1 differential equations are (cf. Bell and Glasstone /2,p.184/):

$$\begin{aligned} \nabla \cdot J_g + \sigma^{rem}_g \phi_g &= \sum_{g'<g} \sigma^{o}_{g'\to g} \phi_{g'} + \frac{1}{k_{eff}} \chi_g \sum_{g'} \nu\sigma^{fis}_{g'} \phi_{g'} \\ \nabla\phi_g + 3\sigma^{1}_g J_g &= \sum_{g'<g} \sigma^{1}_{g'\to g} J_{g'} \,. \end{aligned} \tag{11}$$

The angular flux is then given by

$$\phi(r,\Omega) = \frac{1}{4\pi} (\phi(r) + 3\Omega \cdot J(r)). \tag{12}$$

Volume-integrated difference equations for the P_1 equations are commonly derived as follows. (Cf. Bell and Glasstone /2,pp.137ff./).

We consider the mesh points r_{k-1}, r_k, r_{k+1} as in Section 1, the midpoints $r_{k\pm1/2}$, and $h = r_k - r_{k-1}$, $h' = r_{k+1} - r_k$. Here we treat the general case $h \neq h'$ with cross sections discontinuous at r_k. The first step is to integrate the $\nabla \cdot J$ equation from $r_{k-1/2}$ to r_k:

$$\int_{r_{k-1/2}}^{r_k} r^{n-1} dr: \frac{1}{r^{n-1}} \frac{d}{dr} \left(r^{n-1} \frac{d}{dr} J\right) + \sigma^{rem}\phi = s^o$$

$$r^{n-1} J \Big|_{r_{k-1/2}}^{r_k} + \int_{r_{k-1/2}}^{r_k} \sigma^{rem}\phi r^{n-1} dr = \int_{r_{k-1/2}}^{r_k} s^o r^{n-1} dr$$

Here s^o is the net source for this group, whose group index g has been suppressed. Now we approximate $\sigma^{rem}\phi$ and s^o by their values at r_k, and take

$$\int_{r_{k-1/2}}^{r_k} r^{n-1} dr = \frac{1}{n} (r_k^n - r_{k-1/2}^n) = v_{k-}$$

where $k-$ indicates r_k approached from the left; this leads to:

$$r_k^{n-1} J_k - r_{k-1/2}^{n-1} J_{k-1/2} + \sigma_{k-}^{rem} \phi_{k-} v_{k-} = s_{k-}^o v_{k-} . \qquad (13)$$

In the same way we get to the right of r_k

$$r_{k+1/2}^{n-1} J_{k+1/2} - r_k^{n-1} J_{k+} + \sigma_{k+}^{rem} \phi_{k+} v_{k+} = s_{k+}^o v_{k+} . \qquad (14)$$

Now the second of the P_1 equations (11) can be used to give an approximation for J at $r_{k\pm1/2}$. This is obtained by approximating

$(\nabla\phi)_{k-1/2}$ by the simple central difference.

$$(\phi_k - \phi_{k-1})/h + 3\sigma^1_{k-1/2}\, J_{k-1/2} = 3\, s^1_{k-1/2}.$$

Then setting $D = 1/(3\sigma^1)$, we have

$$D_{k-1/2}\,(\phi_k - \phi_{k-1})/h + J_{k-1/2} = 3D_{k-1/2}\, s^1_{k-1/2} \qquad (15)$$

Now we can eliminate the J's. First we add equations (13) and (14) to obtain

$$r^{n-1}_{k+1/2}\, J_{k+1/2} - r^{n-1}_{k-1/2}\, J_{k-1/2} + (\sigma^{rem}_{k-}\, v_{k-} + \sigma^{rem}_{k+}\, v_{k+})\phi_k$$

$$= s^o_{k-}\, v_{k-} + s^o_{k+}\, v_{k+}$$

since $\phi_{k+} = \phi_{k-}$ and $J_{k+} = J_{k-}$ by the flux and current continuity conditions. Now using the $\nabla\phi$ difference equation (15) twice we eliminate the two remaining J's and get

$$r^{n-1}_{k-1/2}\, D_{k-1/2}\,(\phi_k - \phi_{k-1})/h - r^{n-1}_{k+1/2}\, D_{k+1/2}\,(\phi_{k+1} - \phi_k)/h'$$

$$+ (\sigma^{rem}_{k-}\, v_{k-} + \sigma^{rem}_{k+}\, v_{k+})\phi_k = s^o_{k-}\, v_{k-} + s^o_{k+}\, v_{k+} \qquad (16)$$

$$+ 3r^{n-1}_{k-1/2}\, D_{k-1/2}\, s^1_{k-1/2} - 3r^{n-1}_{k+1/2}\, D_{k+1/2}\, s^1_{k+1/2}$$

This represents a three-point difference equation for the ϕ_k in terms of the sources s^o_k, $s^1_{k\pm1/2}$. Left and right boundary conditions (involving J) can be derived using either (13) or (14) together with (15). For example, the boundary condition $J + \alpha\phi = 0$ at the left is first used to eliminate J_k from (14):

$$r_{1/2}^{n-1} J_{1/2} - r_o^{n-1} \alpha\phi_o + \sigma_o^{rem} \phi_o v_{o+} = s_o^o v_{o+} \quad ;$$

then applying (15) yields

$$-r_{1/2}^{n-1} D_{1/2} (\phi_1 - \phi_o)/h - r_o^{n-1} \alpha\phi_o + \sigma_o^{rem} \phi_o v_{o+} \tag{17}$$

$$= s_o^o v_{o+} - 3r_{1/2}^{n-1} D_{1/2} s_{1/2}^1$$

The resulting tri-diagonal system of equations for the ϕ_k can be solved as usual by Gaussian elimination. As noted in Stewart /7/, with the IBM System 360 one should perform the elimination itself in double precision, although the solution may be stored in single precision.

The source s^o consists of fission production and inscatter; s^1 is the first moment of inscatter. With down-scattering only, the multigroup calculation proceeds for group g by inverting equation (16) for ϕ_g; this ϕ_g is used to complete scattering in group $g+1$ in s_{g+1}^o. Using equation (15) one can then retrieve the current J_g in group g, which is used to complete s_{g+1}^1 in the next group. Once s_{g+1}^o and s_{g+1}^1 are calculated, the equations (16) can be inverted for group $g+1$.

The necessary recovery of J_g via equation (15) involves a numerical differentiation of ϕ_g. However, the Gaussian elimination amounted to integrating twice to arrive at ϕ_g, so it should be possible to avoid the numerical differentiation of ϕ_g by saving the difference equation coefficients as they are after the first integration (forward elimination) but before the second (backward substitution). Indeed, at this point the three-point equations would be reduced by elimination to the form

$$E_k \phi_k + C_k \phi_{k+1} = G_k$$

(cf. Stewart /7, p.7/). It turns out that $E_k \simeq -C_k$ for $h = h' < L$ (= diffusion length). Therefore if one saves the coefficients at this intermediate stage, $\Delta\phi$ can be easily found. Once the solution ϕ_k is found, one goes back and adjusts G_k above by the small amount $(C_k + E_k)\phi_k$ to get

$$C_k(-\phi_k + \phi_{k+1}) = G_k - (C_k + E_k)\phi_k$$

or

$$(\phi_{k+1} - \phi_k)/h = \left[G_k - (C_k + E_k)\phi_k\right]/(C_k h).$$

This value is then substituted into equation (15) to find $J_{k\pm 1/2}$ for group g.

Notice that the P_1 difference equation scheme just outlined always uses ϕ at interval endpoints $(\phi_{k-1}, \phi_k, \phi_{k+1})$ and J at interval midpoints $(J_{k\pm 1/2})$. This seems natural and convenient for carrying through the fission power iterations, as s^o_g, found from fluxes at endpoints, is needed at endpoints, while s^1_g is found at midpoints and used at midpoints. For final output, however, it is more convenient to have both flux and current values at interval endpoints. One could imagine an interpolation scheme for finding J_k from $J_{k\pm 1/2}$; but it is also possible to find J_k in a manner which is fully consistent with our volume-integrated difference equations. To do this we simply rewrite equation (13):

$$J_k = (r^{n-1}_{k-1/2}\, J_{k-1/2} - \sigma^{rem}_{k-}\, v_{k-}\, \phi_k + s^o_{k-}\, v_{k-})/r^{n-1}_k. \qquad (18)$$

(Such a procedure has the extra benefit of giving exactly those values of J at the left and right ends which were implicity used in the approximate boundary conditions.) This shifting of currents values is performed in MANDI after completion of the last outer iteration. To this end the source terms s^o_g for each group must be saved during the last iteration. (Actually MANDI writes on a scratch file the inscatter; fission source is easily added to this.)

Storage Strategies

At this point we would like to mention something about the use of core storage by the program MANDI. The strategy is largely determined by the number of energy groups for which the program was designed (200-300). With a relatively full lower triangular scattering matrix it is not practical to insist that all cross sections be in core at all times. Thus a buffer area is reserved for reading in scattering cross sections as needed. Furthermore one cannot prepare all difference equation coefficients in advance and store them in core; therefore the group-independent terms $v_{k\pm}$ and $r^{n-1}_{k\pm 1/2}/h$ are stored and combined with D_g, σ^{rem}_g only as the individual group is about to be solved. (This does not noticeably slow the calculation, since the time spent summing down-scattering contributions predominates.)

On the other hand, it does seem necessary to hold all the group fluxes in core at all times, since the scattering matrix can be expected to be relatively full. Thus MANDI does require one word of core storage for flux at each space-energy point. Some space can be saved by using the same area for building scattering source terms. During calculation of ϕ_g, the rows of this storage area corresponding to groups $1,2,\ldots,g-1$ hold the fluxes already found for these groups; the rows for groups $g+1,\ldots,G$ are free for the partially completed sums of scattering into these groups from groups of higher energy. (Due to the structure of the standard Karlsruhe cross section file format, the scattering contribution of ϕ_g <u>into</u> all lower energy groups is most conveniently added in as soon as ϕ_g is found. For the adjoint problem, on the other hand, the scattering matrix is transposed, and in this case it is convenient to calculate scattering into group g <u>from</u> all lower energy groups immediately before ϕ_g is to be solved.)

The currents J_g will not be needed during a simple calculation in diffusion approximation, since in this case the first moment of scattering is suppressed. Thus MANDI only needs core storage for ϕ_g in this case and not for J_g. In the P_1 approximation, however, additional core storage of one word per space-energy point is needed for J_g; as with ϕ_g, the current scattering sources may overlap

the J_g themselves. MANDI also requires current storage in core for diffusion calculations in which currents and balances are to be printed; in this case the extra current storage area is needed only during the final iteration, and could probably be avoided by reprogramming.

Neutron Balance Equation

At the end of each MANDI calculation the user may ask that a detailed reaction rate balance equation be printed for each group and zone. This amounts to breaking up the first of the P_1 equations (11) into physically interesting terms and using the final fluxes and currents to calculate the volume integral of each term over each zone. If the terms are added according to the first P_1 equation, the theoretical result, or balance, is zero. In MANDI the volume integrals are calculated numerically in a way which is consistent with the volume-integrated difference equations (16). Therefore the balances printed will deviate from zero only due to iteration error (i.e. outer iterations not exactly converged) and to roundoff error in calculating the balances themselves.

The first component of the balance equation to be printed is leakage. The current leakage out of a zone Z_i is

$$\int_{Z_i} \nabla \cdot J \, dV = \int_{\partial Z_i} J \cdot n \, dS.$$

The surface integral in one-dimensional problems is over the left and right ends of the linear zone:

$$= -J_\ell A_\ell + J_r A_r \quad ,$$

with surface area $A_\ell = 1$ for slab, $A_\ell = 2\pi R_\ell$ for cylinder, and $A_\ell = 4\pi R_\ell^2$ for sphere geometry. In the printout, each net current J_ℓ, J_r is further subdivided into inward and outward currents found from (12); letting $H_+(H_-)$ denote the unit hemisphere of positive (resp. negative) directions with respect to increasing r, we find

$$J_{\ell,in} = \frac{1}{4\pi} \int_{H_+} \Omega\phi(R_\ell) + 3\Omega(\Omega \cdot J(R_\ell))\, d\Omega$$

$$= \phi_\ell/4 + J_\ell/2 \qquad (19)$$

$$J_{\ell,out} = \frac{1}{4\pi} \int_{H_-} \Omega\phi(R_\ell) + 3\Omega(\Omega \cdot J(R_\ell))\, d\Omega$$

$$= \phi_\ell/4 - J_\ell/2$$

where of course $J_\ell = J_{\ell,in} - J_{\ell,out}$.

In slab and cylinder geometries there may be an additional leakage due to a transverse buckling. This buckling enters the first of the P_1 equations via a term $D_g B^2 \phi_g$ added to the σ^{rem} term; the resulting leakage is found to be $\int D_g B^2 \phi_g \, dV$. (At this point we remark that numerical volume integration for balances is performed consistently with the difference equations, e.g. for flux by summing $\phi_k(v_{k-} + v_{k+})$ across the zone.) The current leakage plus buckling leakage gives total leakage.

In additon to the total leakage, the following terms appear in the balance equation:

$$\int dV: \underbrace{(\nabla \cdot J_g + D_g B^2 \phi_g)}_{\text{total leakage}} + \underbrace{\sigma_g^{capt}\phi_g}_{\text{capture}} + \underbrace{\sigma_g^{fis}\phi_g}_{\text{fission removal}} + \underbrace{\sigma_g^{out}\phi_g}_{\text{out-scatter}}$$

$$\underbrace{- \sum_{g'<g} \sigma^o_{g'\to g}\, \phi_{g'}}_{\text{inscatter}} \underbrace{- \frac{1}{k_{eff}} \chi \sum_{g'} \nu\sigma^{fis}_{g'}\, \phi_{g'}}_{\text{fission production}} = \text{balance} \qquad (20)$$

Tchebysheff Acceleration

The outer iterations in MANDI are accelerated by the well-known Tchebysheff extrapolation technique applied to the fission source; for a detailed review of this method see for example Stewart /7/. Here we make only a few documentary remarks. During the first few outer iterations the dominace ratio is repeatedly estimated; when this estimate converges to within .01 difference between successive iterations, Tchebysheff acceleration begins. Until that point, overrelaxation is used; after that, successive Tchebysheff extrapolations of increasing order are calculated by a recursion formula, always using the single last estimate of the dominance ratio.

Reduction of the P_1 Equations

Finally we would like to derive a method of reducing the multigroup P_1 equations to a form of multigroup diffusion problem. Although this idea was not incorporated into MANDI, it might be useful under certain conditions. We remark that a similar reduction of mono-energetic P_3 equations to two diffusion equations is given in Gelbard /4,pp. 301 ff./ for slab geometry. Here we are specifically interested in the multigroup problem which is spatially heterogeneous.

The idea of the derivation is to eliminate the first moment equation with the P_1 equations taken for all groups together. We do this for regions of constant material cross sections, and get multigroup diffusion equations with new transfer cross sections. We then consider the necessary changes in continuity conditions at interfaces where the P_1 cross sections have jump discontinuities.

The P_1 equations to solve are

$$\nabla \cdot J_g + \sigma_g^{rem}\phi_g = \sum_{g'<g} \sigma^o_{g'\to g}\phi_{g'} + \frac{1}{k}\chi_g \sum_{g'} \nu\sigma^{fis}_{g'}\phi_{g'}$$

$$\nabla\phi_g + 3\sigma^1_g J_g = 3 \sum_{g'<g} \sigma^1_{g'\to g} J_{g'} \,. \tag{21}$$

Taking the divergence of the second equation (within a region of constant cross sections) gives

$$\nabla \cdot \nabla\phi_g + 3\sigma_g^1 \nabla \cdot J_g = 3 \sum_{g'<g} \sigma_{g'\to g}^1 \nabla \cdot J_{g'} \quad ,$$

and, taking $D_g = 1/(3\sigma_g^1)$ as usual, we can substitute this into the first P_1 equation to eliminate $\nabla \cdot J_g$ from the left:

$$- D_g \nabla^2 \phi_g + \sigma_g^{rem} \phi_g = - 3D_g \sum_{g'<g} \sigma_{g'\to g}^1 \nabla \cdot J_{g'} + \sum_{g'<g} \sigma_{g'\to g}^o \phi_{g'}$$

$$+ \frac{1}{k} \chi_g \sum_{g'} \nu\sigma_{g'}^{fis} \phi_{g'} .$$

Of course we have now introduced $\nabla \cdot J_{g'}$, $g'<g$, on the right, but this can be removed once and for all by applying the first P_1 equation again:

$$- 3D_g \sum_{g'<g} \sigma_{g'\to g}^1 \nabla \cdot J_{g'} = 3D_g \sum_{g'<g} \sigma_{g'\to g}$$

$$\left[\sigma_{g'}^{rem} \phi_{g'} - \sum_{g''<g'} \sigma_{g''\to g'}^o \phi_{g''} - \frac{1}{k} \chi_{g'} \sum_{g''} \nu\sigma_{g''}^{fis} \phi_{g''}\right]$$

$$= 3D_g \sum_{g'<g} \sigma_{g'}^{rem} \sigma_{g'\to g}^1 \phi_{g'} - \underbrace{3D_g \sum_{g'<g} \sum_{g''<g} \sigma_{g''\to g'}^o \sigma_{g'\to g}^1 \phi_{g''}}_{S}$$

$$- \frac{1}{k} 3D_g \sum_{g'<g} \sum_{g''} \sigma_{g'\to g}^1 \chi_{g'} \nu\sigma_{g''}^{fis} \phi_{g''} .$$

We now find it convenient to interchange g' and g'' everywhere. Next, for the double sum in S recall that

$$\sum_{g''<g} \sum_{g'<g''} = \sum_{g'<g} \sum_{g'<g''<g} .$$

We can now carry through the substitution for $\nabla \cdot J_{g'}$ as announced above; after rewriting the double sum we get

$$-D_g \nabla^2 \phi_g + \sigma_g^{rem} \phi_g = \sum_{g'<g} \left[\sigma^o_{g' \to g} (1 - 3D_g \sum_{g'<g''<g} \sigma^1_{g'' \to g}) + 3D_g \sigma^1_{g' \to g} \sigma^{rem}_{g'} \right] \phi_{g'}$$

$$+ \frac{1}{k} \left[\chi_g - 3D_g \sum_{g''<g} \sigma^1_{g'' \to g} \chi_{g''} \right] \sum_{g'} \nu \sigma^{fis}_{g'} \phi_{g'} . \qquad (22)$$

It is then proposed to solve these equations instead of the P_1 equations (21) above. The terms in brackets can be evaluated before the calculation begins, and stored for use as substitute cross sections. The calculation would then proceed just like a diffusion calculation; in particular there would be no need to handle currents explicitly at all space intervals. Thus the core storage and execution time would be nearly the same for P_1 calculations by this method as for the usual diffusion calculation (and not doubled, as in MANDI). The only extra effort, in addition to the substitute cross sections, would be a special handling of interface continuity conditions, as follows.

In P_1 theory, the usual conditions

$$[\phi_g] = [J_g] = 0 \quad , \quad [\ ] = \text{jump across interface},$$

are imposed. To translate continuity of J_g, which has been eliminated, into a condition for ϕ_g, we can use the second P_1 equation at the

interface. For $g = 1$ we have simply

$$\nabla\phi_1 + 3\sigma_1^1 J_1 = 0,$$

so for $[J_1] = 0$ we can substitute $[D_1\nabla\phi_1] = 0$. Furthermore we can recover the value of J_1 at the interface and save it.

For $g>1$ we suppose the groups $1,2,\ldots,g-1$ have been solved, and currents $J_{g'}$ for those groups at the interface have been stored. Then the jump in the right side of the second P_1 equation is easily found. We therefore replace the condition $[J_g] = 0$ by the condition

$$[D_g\nabla\phi_g] = [3D_g \sum_{g'<g} \sigma_{g'\to g}^1 J_{g'}].$$

Then one simply finds the value of J_g at the interface, stores it for use in lower groups, and proceeds. In this way one need only consider current values at the material interfaces.

Flowchart for MANDI

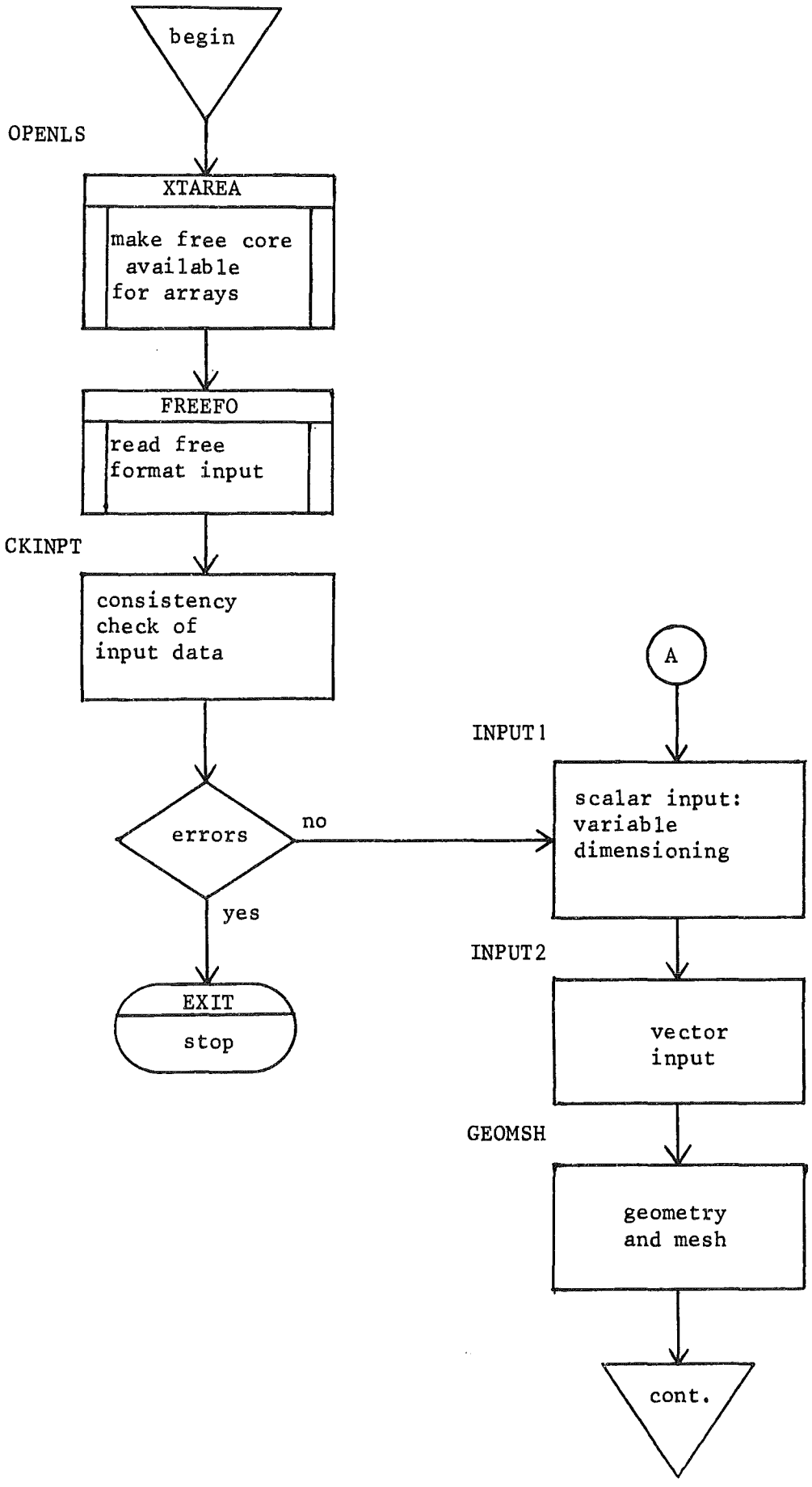

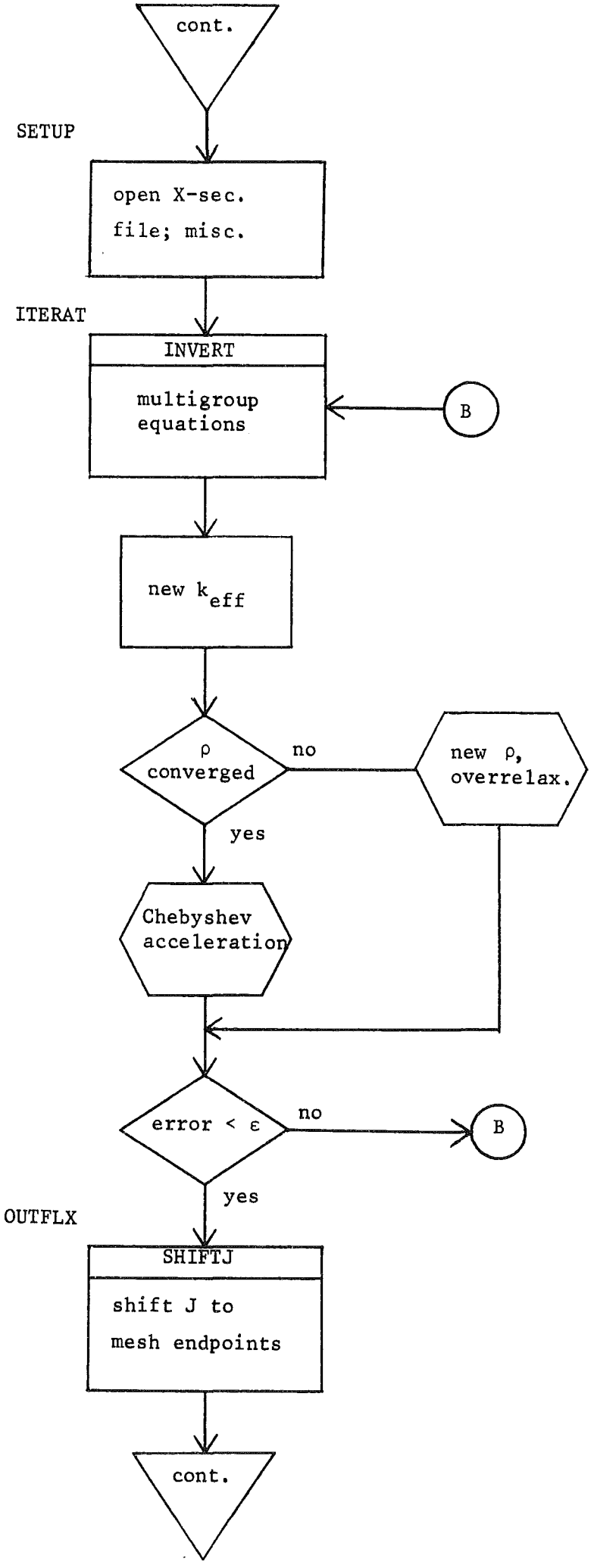
cont.
SETUP
open X-sec.
file; misc.
ITERAT
INVERT
multigroup
equations
B
new k_{eff}
ρ
converged
no
new ρ,
overrelax.
yes
Chebyshev
acceleration
error < ε
no
B
yes
OUTFLX
SHIFTJ
shift J to
mesh endpoints
cont.

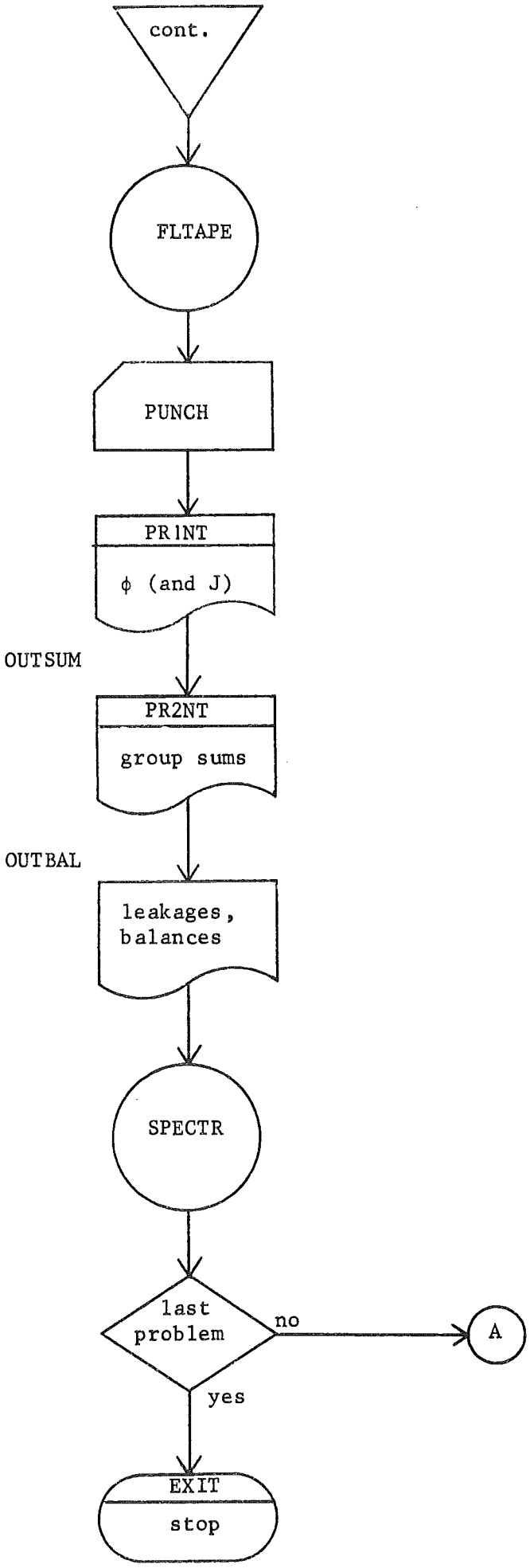
cont.
FLTAPE
PUNCH
PRINT
ϕ (and J)
OUTSUM
PR2NT
group sums
OUTBAL
leakages, balances
SPECTR
last problem
no
A
yes
EXIT
stop

INVERT

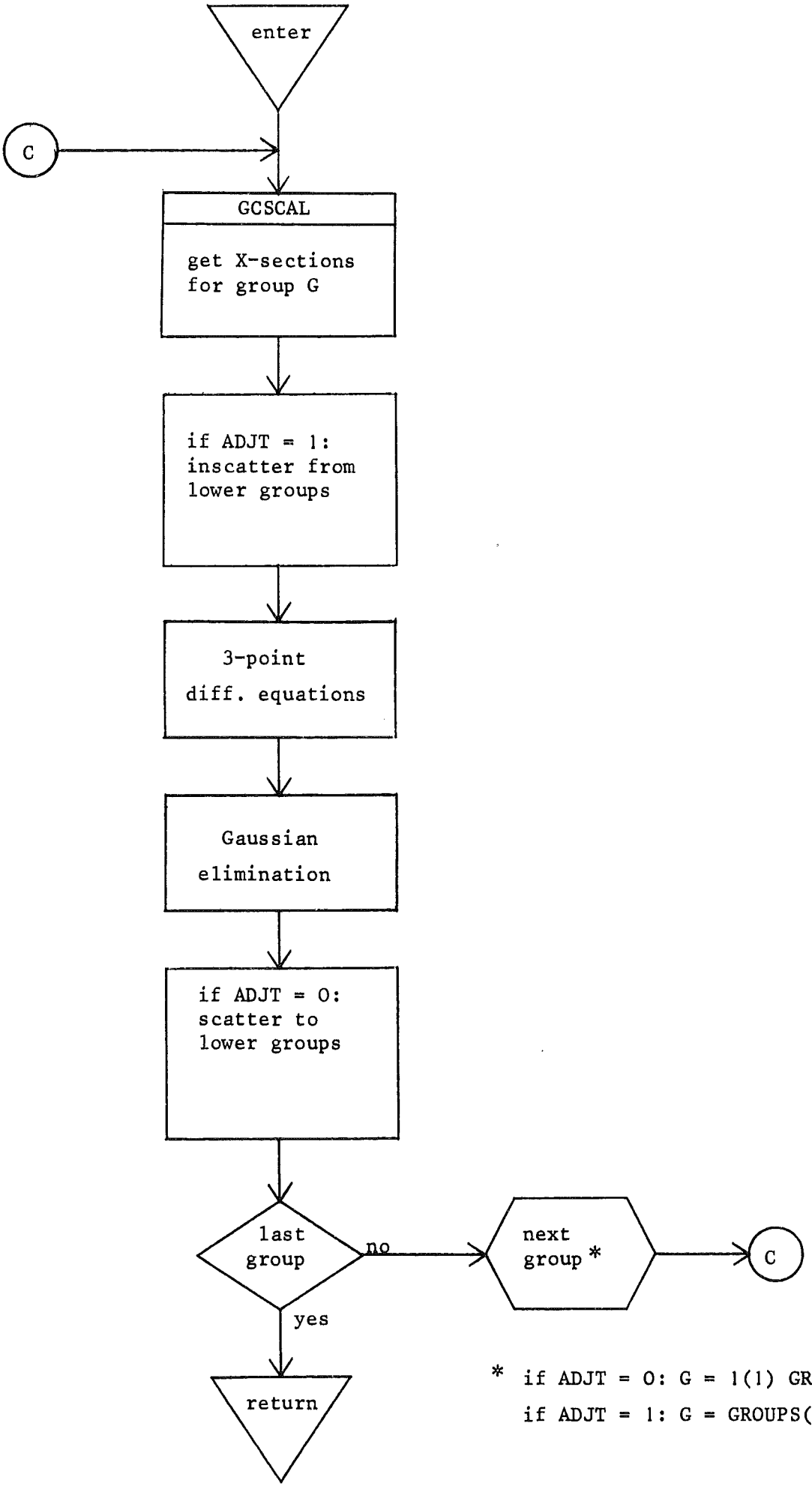
enter
C
GCSCAL
get X-sections for group G
if ADJT = 1: inscatter from lower groups
3-point diff. equations
Gaussian elimination
if ADJT = 0: scatter to lower groups
last group
no
next group *
C
yes
return
* if ADJT = 0: G = 1(1) GROUPS
if ADJT = 1: G = GROUPS(-1)1

Section 3. User's Information

This section contains information about the Fortran IV program MANDI relating to normal program use, and some details about the Karlsruhe implementation. First we describe program options available to the user; then the format of input, output, and intermediate data handling; finally we remark on program execution.

Options

In its present form MANDI performs a sequence of one or more one-dimensional multigroup calculations. Each calculation is described by a complete card input, and multigroup cross sections for each calculation are assumed to be available. Each calculation can be performed in a number of different ways; the options include:

(a) P_1 or diffusion approximation, that is, the P_1 multigroup equations (11) of Section 2, or the diffusion equations obtained by ignoring scattering in first moments ($\sigma_1^{g'\to g}$) and choosing $D_g = 1/(3\sigma_g^{tr})$;

(b) k-eigenvalue or external source calculation (in a subcritical system), using equations (11) of Section 2 to determine the fundamental k-eigenmode, or setting $k=1$ and determining the flux resulting from an added external source term, $s_g(r) = R(r) \cdot \Sigma(g)$, where R and Σ are given in the input;

(c) the neutron flux or the adjoint equations, i.e. those in (11) or the adjoint equations obtained by interchanging g' and g in the scattering and fission terms, and replacing J by $-J$ (cf. Bell and Glasstone /2,p.272/);

(d) without or with special recursive treatment of the elastic scattering by hydrogen, depending on what cross sections are supplied; in the latter case,

$$\sigma^{o}_{g'\to g} = \sigma^{o,noH}_{g'\to g} + \sigma^{o,H}_{g'} \cdot (\Delta E)_g$$

$$\sigma^{1}_{g'\to g} = \sigma^{1,noH}_{g'\to g} + \sigma^{1,H}_{g'} \cdot (\tfrac{2}{3}\Delta E^{3/2})_g$$

where the H terms, having separated g'- and g-dependence, can be calculated recursively (as for fission source); calculation time is saved if a large number of entries in the no-H scattering matrices vanish;

(e) buckling and time eigenvalue may be specified, which amounts to replacing σ_g^{rem} by

$$\sigma_g^{rem} + D_g B^2 + \alpha/V_g \quad ,$$

where V_g is the average neutron velocity in group g; the quantity B^2 may be a universal buckling, or may be group-dependent or group- and zone-dependent; if the net term becomes negative, a warning will be printed, as the solution method will not necessarily be stable in this case;

(f) geometry may be slab, cylinder, or sphere;

(g) boundary conditions at the left and right ends may be either $\phi=0$, or $J=0$ (symmetry), or diffusin boundary condition, i.e. $\phi \pm 2.13\, J = 0$ (+ at left, - at right).

All of these options may be combined in any manner. A number of options for output exist and are described below.

Input Description

Basic input to MANDI consists of cards in so-called free format which are read from the normal card input stream. A subroutine in the Karlsruhe system library called FREEFO reads the free-format input from standard unit 5 and transforms the data to unformatted records which are stored on unit 1, and later read by MANDI. The user must reserve a scratch file on unit number 1 for this purpose.

In free format conventions, a card whose first data character is punched in column 1 signals the beginning of a new record; beyond this, any arrangement of data in columns 1-71 is allowed (provided only that no data item contains internal spaces, and at least one space separates each item from the next). In the description below, a new record is signaled by the K's at the left; S-numbers just indicate a branch point in the description. Items in quote marks are copied into

the input, quote marks included; the others are variable names whose values should be supplied as indicated. Variable names are usually the internal FORTRAN names; note that the FORTRAN type convention (I-N = integer) is not followed, but here the types should be clear.

Before using this input description please read all of Section 3 and the end of Section 1 ("Rules of Thumb").

K1 'INPT'

K2

P1	= 0	for diffusion
	= 1	for P_1 approximation
INH	= 0	for k-eigenvalue calculation
	= 1	for external source
ADJT	= 0	for neutron flux
	= 1	for adjoint problem
HSPEC	= 1	if cross sections are available for recursive treatment of H-scattering,
	= 0	otherwise
GCFILE	unit number of group cross sections arranged in SIGMN structure (see below)	
FLTAPE	= 0	no flux tape writen
	> 0	unit number for writing geometry, final fluxes (and currents if JPR=1, in K24)
SCRTCH	= 0	no scratch unit
	> 0	scratch unit number used for final inscatter; must be provided if JPR=1 in K24 or balances or leakages are desired.

K3

GROUPS	number of energy groups	
ZONES	number of (homogeneous) spatial zones	
GEOM	= 1	for slab
	= 2	for cylinder
	= 3	for sphere
LBC	indicates type of left boundary condition:	
	= 1	for zero flux
	= 2	for zero current
	= 3	for diffusion boundary condition

RBC type of right boundary condition, as above (see also option (g) above)

ERRK iteration convergence criterion for k_{eff} (or for total fission source if INH=1)

ERRFS iteration convergence criterion for point values of fission source; if zero is given, set equal to 10 x ERRK.

ALPHA time constant α

K4 'ITER'

ITMAX
- > 0 maximum number of outer iterations
- < 0 exact number of iterations (In this case ERRK and ERRFS are ignored)
- = 0 or absent: maximum = 30

K5 'GEOM'

K6 LEFT(1) real coordinate of left edge ($\geq$ 0 if GEOM > 1)

(MIX(I),BASIC(I),LEFT(I+1),I=1,ZONES)

for each zone: mixture identification number (in SIGMN block), number of basic mesh steps, coordinate of right boundary

S7 if INH=0: K8, then S10

if INH=1: K9, then S10

K8 'FSSC'

TYPES
- = 1: fission source guess given at ends of each zone and interpolated linearly
- = 2: fission source given at each point

K9 'EXSC'

TYPES
- = 1: space dependence of external source given at ends, to be linearly interpolated
- = 2: space dependence of external source given at each point

S10 if TYPES=1: K11, then S13; = 2: K12, then S13

K11 (LINSC(1,I), LINSC(2,I), I=1, ZONES)
for each zone, source at left and right end

K12 (PTSC (I), I=1, PTZ)
source at each refined space point, counting zone interfaces twice

S13 if INH=1: K14

K14 IGR number of groups for which the energy dependence of external source is given (in other groups, set equal to zero)
(ENRGY(I),I=1,IGR)
energy dependence of external source, for consecutive groups starting with the group of highest energy

K15 'BUCK'
TYPEB = 1,2, or 3 for type of bucking input

S16 if TYPEB = 1: K17, K20; =2: K18, K20; =3: K19,K20

K17 BUCK universal buckling

K18 (BUCK(I), I=1, GROUPS)
buckling for each zone and group

K19 ((BUCK(I,J), I=1, ZONES), J=1, GROUPS)
buckling for each zone and group

K20 'REFN'

S21 for each end (left and right) of each zone, K22

K22 IRF number of basic intervals to refine ($\geq$ 1)
(REFINE(I), I=1, IRF)
integer refinement factors ($\geq$ 1) for basic intervals starting next to interface and moving toward mid-zone. (cf. examples in Section 1)

K23 'OTPT'

K24 EDIT = 0 no flux printout
= 1 fluxes printed at zone boundaries
= 2 fluxes printed at basic mesh points
= 3 fluxes printed at all points
JPR = 1 print currents also (with same editing), and write them on FLTAPE
= 0 no current output
GRSEL = 0 all groups used in flux printout
= 1 fluxes printed for user-selected groups only
GRSUM = 1 print partial group sums of pointwise fluxes, as requested by user
= 0 no partial group sums
LKG = 1 print zone-group leakages
= 0 no leakage output
BAL = 1 print detailed neutron balance equation for each zone and group
= 0 no balances printed
SPECTR > 0 unit number on which fluxes and leakages are written for later use as group collapsing spectra
= 0 no spectra written
PUNCH > 0 unit number on which the final fission source values are written in punched card format suitable for later use as source guess input
= 0 no fission source written

S25 if GRSEL=1: K26

K26 N number of entries in group selection list (not number of selected groups)
(GRPS(I), I=1,N)
groups selected for flux printout; if a positive number g is followed by a negative -h, this means all groups from g up through h (g<h).

S27 if GRSUM=1: K28

K28 N number of partial group sums
(GRIST(I), GRLAST(I),I=1,N)
for each N, the first and last groups in the range of summation

K29 'END '

S30 if another MANDI problem follows: K1;
otherwise:

K31 'END '

Note that the following blocks may be omitted from the input:
'ITER' , if 30 iterations maximum is acceptable;
'BUCK' (K15-K19), if buckling is zero;
'REFN' (K20-K22), if no local refinement is desired;
'OTPT' (K23-K28), if only k_{eff} and final fission source need be printed.

Cross Section Data

A basic condition for each MANDI calculation is that the effective multigroup cross sections be available on an external file (e.g. disk). The present version of MANDI uses cross sections in a format called SIGMN, which is used at Karlsruhe together with special data handling routines WQORG. For the sake of documentation we give some description of this format.

A set of SIGMN data consists of a label record, a record of information about cross sections in the particular set, followed by one record for each group containing the cross sections in the various material mixtures for that group. Each type of cross section has an eight-letter left-justified name, which may be one of the following:

DIFKO	D_g	diffusion coefficient for P_1
STR	σ_g^{tr}	$D_g = 1/(3\sigma_g^{tr})$ for diffusion
SREM	σ_g^{rem}	removal cross section
SFISS		fission removal part of σ^{rem}
SCAPT		capture part of σ^{rem}
STOT		total collision cross section ($\sigma_g^{rem} + \sigma_{g\to g}^{o}$)
1/V		inverse of average neutron velocity
CHI	χ_g	fission spectrum
NUSF	$\nu\sigma_{g'}^{fis}$	fission production cross section
SMTOT	$\sigma_{g'\to g}^{o}$	net scattering cross section
SME1	$\sigma_{g'\to g}^{1}$	first scattering moment
SMTH	$\sigma_{g'\to g}^{o,noH}$	scattering except hydrogen
SME1H	$\sigma_{g'\to g}^{1,noH}$	first scattering moment, except H
SBEH	$\sigma_{g'}^{o,H}$	H scattering per energy interval
SBEH1	$\sigma_{g'}^{1,H}$	first H scattering moment per $E^{3/2}$
DE	ΔE, $\frac{2}{3}\Delta E^{3/2}$	

Different types will be needed for P_1 vs. difusion calculations, and for calculations with or without recursive treatment of hydrogen scattering. The requirements are summarized in the following table:

	without,	with recursive H-scat.	
diff.	STR SMTOT	STR SMTH	SBEH DE
P_1	DIFKO SMTOT SME1	DIFKO SMTH SME1H	SBEH SBEH1 DE

Additional type requirements can be summarized as follows:

always: SREM, CHI, NUSF
if $\alpha \neq 0$: 1/V
for balance output: SCAPT, SFISS, STOT

The cross section data set is controlled by routines in MANDI which are minor modifications of the WQORG routines. There are three entries in the MANDI version: OPENGC which initializes the routines, GCSCAL which delivers scalar types, and GCVECT which delivers vector types, i.e. scattering cross sections which consist of more than one value for each group and mixture (SMTOT, SME1, SMTH, SME1H, DE). These subroutines are called as follows:

OPENGC (BFLENG, BUF, BUF, GCFILE, MIXES)
- BUF is a buffer area to be used for reading the cross sections; OPENGC initializes by reading in as many groups as will fit into BUF, and leaves room for the remaining groups to be read one at a time when needed.
- BFLENG gives the number of words in BUF.
- GCFILE is the external unit number for cross section data.
- MIXES is a return argument for the number of material mixtures on the data file, and is needed later to locate vector-type data.

GCSCAL (G, TYPE, PTR)
- G is the group number of requested data.
- TYPE is the eight-letter name of a scalar data type to be located.
- PTR is a return argument pointer for the desired cross section data; the value for mixture M ($1 \leq M \leq$ MIXES) is to be found at BUF(PTR + M).

GCVECT (G,TYPE, PTR, FG, LG)
- G is the requested group <u>from</u> which scattering occurs.
- TYPE is the vector (scattering) type name.
- FG and LG are return values, the first and last groups <u>into</u> which scattering occurs.
- PTR is the return argument pointer; the cross section from group G to group H for mixture M is found at BUF(PTR + (H-FG) MIXES + M). In case TYPE=DE, ΔE_G is found at BUF(PTR + 1), with $\frac{2}{3}(\Delta E^{2/3})_G$ at BUF(PTR + 2).

Program Output

MANDI output consists of printed output and several files which may be stored on disk, magnetic tape, or punched cards for later use. The output can be selected and edited to a considerable extent by the user.

The printed output (for a sample see Appendix B) always begins with an echo check of the card input for all problems. Then the output for each problem appears. First comes a heading which describes the problem (geometry, options), followed by a history of outer iterations. Next the final overall values are printed: for external source problems, the integral of the fission source; for k-eigenvalue problems, the final estimate of k_{eff} together with upper and lower bounds for iteration error (not discretization error); in either case the final fission source is printed at each point.

Thereafter all output is optional. Fluxes may be printed for all groups at each point; or if desired, only at basic mesh points, or only at zone endpoints. Furthermore, the user may opt to print fluxes only for selected groups. If fluxes are printed, the user may ask for currents to be printed with the same editing. For external source problems flux and current are not renormalized; for k-eigenvalue problems, equations (11) are renormalized so that the fission source ($\Sigma_{g'} \nu\sigma_{g'}^{fis} \phi_{g'}$) has norm (i.e. volume integral) equal to one. The fluxes and currents may also be printed in partial group sums, with summation ranges given by the user.

The final printed output may contain an evaluation of the leakages and a detailed neutron balance equation for each zone and each group. Each zone is treated in a separate output segment, containing the components of leakages for all groups first, then the detailed zone balance equation for all groups (refer back to Section 2). Either leakage components or balance equations can be suppressed.

Other output options are available to preserve results of a calculation for later re-use. File size can be figured from the following descriptions; according to names used in the input description, the units are:

FLTAPE - This unit, if supplied, receives a record containing geometry information, followed by the group fluxes, and then by group currents if

JPR=1. For simplicity and compatibility, all flux (and current) values at refinement mesh points are dropped, and only values on the zone-wise uniform basic mesh are written. Output is unformatted. Formally, if R indicates a separate output record, the output to FLTAPE is:

R1	I	3 x (ZONES + 1), number of items in R1
	J	= GEOM - 1
	ZONES	integer number of zones
	LEFT(1),	as in input description
	(BASIC(Z),MIX(Z), LEFT(Z+1), Z=1, ZONES)	

S2 for each group G=1, GROUPS: R3

R3 (FLUX(I,G), I=1,BPTS)
flux at basic mesh points only, interface points counted twice

S4 if JPR=1, for each group G=1, GROUPS: R5

R5 (CRNT(I,G), I=1, BPTS)
current, as above.

SCRTCH - This unit is intended primarily as an intermediate storage for MANDI, but its contents may be of interest to the user. During the last outer iteration, if this unit is available, MANDI writes the in-scatter for each group (i.e. $\Sigma_{g'<g} \sigma^{o}_{g'\to g} \phi_{g'}$), one record per group. This includes recursive H terms, but not the external source. For an adjoint calculation, scattering cross section indices are transposed, the sum is for $g'>g$, and groups are written in reverse order. The group number is always included at the beginning of each record; values are written for all refined mesh points.

The total in-scatter for each group is needed for the current shifting scheme (cf. Section 2), and for leakage and balance calculations. Therefore SCRTCH must be supplied if JPR=1 or if BAL or LKG=1.

S1 for all groups: R2
(G=1, GROUPS for flux, in reverse order for adjoint calculations)

R2 G group number
(SCATSC(I,G), I=1, PTZ)
in-scatter on last iteration at all refined mesh points, interfaces counted twice.

SPECTR - Spectra for later use in group collapsing can be deposited on this unit. These spectra are results of the balance calculations, but SPECTR may be used even without balance printout. The spectra are zone integrals of flux for each group, and zone integrals of $\nabla \cdot J$ (i.e. current leakage) for all groups.

Note that the leakages written on SPECTR do not include buckling leakages. The use of leakages as condensation spectra is in any case somewhat risky, since they are not necessarily positive; $\nabla \cdot J$-weighted collapsing should be done only with great care.

S1 for each group G=1, GROUPS: R2

R2 (FLINT(Z,G), Z=1, ZONES)
flux integral in each zone

S3 for each group G=1, GROUPS: R4

R4 (LK(Z,G), Z=1, ZONES)
current leakage for each zone.

PUNCH - If a problem is to be repeated in similar form and with the same space mesh, the final fission source can be punched out on cards for later use as an initial guess. The values of the final fission source at each refined mesh point are punched in a card format which may be used directly as input under the heading 'FSSC'.

Remember that for any calculation unit number 1 must always be provided as a scratch file for free format input.

Program Execution

Finally we would like to add a few remarks about the workings of MANDI in its present implementation. MANDI currently resides in the Karlsruhe nuclear program library as a stand-alone code. MANDI was written in Fortran IV and translated and linked into a form executable by the IBM System 360 Fortran H (Extended) loader.

After being loaded into main core storage, MANDI calls a Karlsruhe library subroutine FREESP to find how much free core storage is available within the job region, subtracts room for input-output buffers, and then calls a library subroutine XTAREA which, via GETMAIN, opens the free core storage in a block for variably dimensioned arrays. All arrays will be redimensioned to fit compactly for each new calculation.

Next MANDI calls the library subroutine FREEFO to read the free format input and deposit it in unformatted record structure on unit 1. The entire MANDI input is immediately subjected to a consistency check by the MANDI subroutine CKINPT. If an error is detected, a printed message identifies the offending card; CKINPT tries to continue the consistency check, but no calculation will be attempted.

After a successful input check there are four reasons for which MANDI might terminate: (1) core storage region too small; (2) error in using the cross section file; (3) external source calculation determined to be supercritical; (4) system interrupt due to undetected input error, unforseen internal error in MANDI, or system failure. In the first three cases MANDI prints a self-explanatory message before abandoning the job.

Core storage is assigned automatically by MANDI within the given job region. Arrays are dimensioned anew for each problem, and all remaining free storage is given to OPENGC for the cross section buffer. If core region is sufficient, the division into array area and cross section buffer is printed out. If not, MANDI tries to estimate the minimum extra amount needed. With the present program overlay structure, total basic requirements can be estimated by the formula (in System 360 bytes).

REGION = 65 K + (GROUPS + 18) x (POINTS + 3 x ZONES) x 4

to which one adds

+ GROUPS x (POINT + ZONES) x 4

in case P1=1 or SCRTCH > 0. As already indicated, any extra core storage will be assigned to hold more cross sections in core. Other than available core storage, there are no limits on the number of points or groups which may be used. (The input consistency check subroutine assumes ZONES $\leq$ 100, but this could easily be increased.)

MANDI execution terminates normally by a CALL EXIT (n). In case n=0, the subroutine EXIT prints a normal end message and executes a STOP statement. If n < 0, an error condition is understood; in this case EXIT will attempt to trigger a core dump by addressing a non-existent core storage location.

The flowchart at the end of Section 2 shows the various subroutines of MANDI in more detail.

References

1. ABRAMOWITZ, M., and I.A. STEGUN: Handbook of Mathematical Functions. Washington, D.C.: National Bureau of Standards, 1964.

2. BELL, G.I., and S. GLASSTONE: Nuclear Reactor Theory. New York: Van Nostrand, 1970.

3. COURANT, R., and D. HILBERT: Methods of Mathematical Physics, Volume II. New York: Interscience, 1962.

4. GELBARD, E.: "Spherical Harmonics Methods: P_L and Double-P_L Approximations", in Greenspan, H., C.N. Kelber, and D. Okrent, Computing Methods in Reactor Physics, New York: Gordon and Breach, 1968.

5. HENNART, J.P.: "Numerical Methods of High Order Accuracy for One-Dimensional Diffusion Equations," Nuc. Sci. Eng. 50, 185-199 (1973).

6. STEWART, H.B.: "Choosing a Spatial Mesh for a One-Dimensional Multigroup Diffusion Calculation," unpublished.

7. STEWART, H.B.: "Alternative Numerical Methods for One-Dimensional Multigroup Diffusion Problems," Report KFK 1856 (1973).

8. STEWART, H.B.: "Error Analysis and Efficient Computation for One-Dimensional Diffusion Problems," Reaktortagung des DAtF in Berlin, 1974.

9. STRANG, G., and G.J. FIX: An Analysis of the Finite Element Method. Englewood Clifts, N.J.: Prentice-Hall, 1973.

10. THIEM, D., and E. KIEFHABER:"Untersuchungen zur Genauigkeit der in Karlsruhe häufig benutzten ein- und zwei-dimensionalen Diffusions-programme", unpublished.

Appendix A: Sample Problem Description

Two sample problems were used for 208-group test calculations; their characteristics are summarized.

I. ZPR-3 Assembly 48

A Pu-U-C-Na system simulating the spectrum of large fast power reactors.

Geometry: spherical

core radius = 45.213 cm

reflector thickness = 30 cm

corresponding symmetric slab:

core half-width = 38.18 cm

reflector thickness = 30.48 cm

transverse buckling = 18.132×10^{-4} cm^{-2}

Material composition (atomic number density, 10^{20} atoms/cm^3):

Element	Core	Blanket
Al	1.09	-
C	207.67	-
Cr	26.81	14.81
Fe	99.85	55.15
Mo	2.06	-
Na	62.31	-
Ni	13.30	7.29
Pu 239	16.45	-
Pu 240	1.06	-
Pu 241	0.11	-
Pu 242	0.004	-
U 235	0.16	0.82
U 238	74.27	383.77

II. SUAK Assembly UH1B

A small subcritical assembly, essentially unreflected, for fast neutron spectrum measurements.

Geometry: axial model calculated as symmetrized slab

core half-width = 16.525

iron plate width = 4.5 cm

aluminum plate width = 3 cm

transverse buckling = 132.20×10^{-4} cm^{-2}

Material composition (atomic number density, 10^{20} atoms/cm^3):

Element	Core	Iron plate	Al plate
Al	42.77		600.0
C	74.42		
Fe	-	844.0	
H	148.84		
Ni	5.69		
U 235	65.46		
U 238	261.08		

For additional information on both problems see E. Kiefhaber and J.J. Schmidt, "Evaluation of Fast Critical Experiments Using Recent Methods and Data," Report KFK 969 (1970).

```
ECHO CHECK OF INPUT DATA

'INPT'
0  0  0  0      20  00  19
208  2  3  2  3  1.E-5  0.  0.
'GEOM'
0.        1   30    45.213
          2   20    75.213
'FSSC'    1
0.33  0.13    0.07  0.
'REFN'
1      1
4      8    4    2    1
2      2    1
1      1
'OTPT'
2   1     0    0     1    1     00     0C
'END '
'END '
```

ONE-DIMENSIONAL MULTIGROUP CALCULATION

DIFFUSION K EIGENVALUE

208 GROUPS 2 ZONES SPHERE GEOMETRY

ZONE	BOUNDARY	MIXTURE	BASIC MESH STEPS,	WIDTH	BOUNDARY CONDITION
	0.0				J = 0
1		1	30	1.5071	
	45.2130				
2		2	20	1.5000	
	75.2130				EXTRAPL.

CONVERGENCE CRITERIA
FOR K EFF = 0.000010
FOR FISSION SOURCE VALUES = 0.000100

GROUP CONSTANTS ASSIGNED 31937 WORDS
OTHER STORAGE = APPROX. (GROUPS + 18) * (POINTS + 3 * ZONES)
PLUS GROUPS * (POINTS + ZONES) FOR CURRENTS
TOTAL = 60671 WORDS

OUTER ITERATIONS

ITERATION= 1, K EFF = 0.774706
ITERATION= 2, K EFF = 0.880121 , AN = 1.26424
ITERATION= 3, K EFF = 0.935427 , AN = 1.24853
ITERATION= 4, K EFF = 0.945506 , AN = 1.26797
ITERATION= 5, K EFF = 0.947674 , AN = 1.27740
ITERATION= 6, K EFF = 0.948210 , AI = 1.27905 , BI = 0.0
CHEBYSHEV ACCELERATION BEGUN, DOMINANCE RATIO = 0.44
ITERATION= 7, K EFF = 0.948323 , AI = 1.33087 , BI = 0.04051
ITERATION= 8, K EFF = 0.948371 , AI = 1.30550 , BI = 0.02068
ITERATION= 9, K EFF = 0.948401 , AI = 1.30499 , BI = 0.02027
ITERATION= 10, K EFF = 0.948408 , AI = 1.30498 , BI = 0.02027
ITERATION= 11, K EFF = 0.948409 , AI = 1.30497 , BI = 0.02027

FINAL ESTIMATE FOR K EFF = 0.948409
0.948404 ≤ K EFF ≤ 0.948411 FOR THIS DISCRETIZATION

NORMALIZED FISSION SOURCE

	NORM = 1/K	NORM = 1	ZONE	RADIUS	UNREFINED MESH	
1	4.61650E-06	4.37834D-06	1	0.0	1	4.37834D-06
2	4.61175E-06	4.37383D-06	1	1.5071	2	4.37383D-06
3	4.59751E-06	4.36032D-06	1	3.0142	3	4.36032D-06
4	4.57383E-06	4.33786D-06	1	4.5213	4	4.33786D-06
5	4.54080E-06	4.30654D-06	1	6.0284	5	4.30654D-06
6	4.49854E-06	4.26646D-06	1	7.5355	6	4.26646D-06

7	4.44721E-06	4.21778D-06	1	9.0426	7	4.21778D-06
8	4.38700E-06	4.16068D-06	1	10.5497	8	4.16068D-06
9	4.31813E-06	4.09535D-06	1	12.0568	9	4.09535D-06
10	4.24084E-06	4.02205D-06	1	13.5639	10	4.02205D-06
11	4.15541E-06	3.94103D-06	1	15.0710	11	3.94103D-06
12	4.06214E-06	3.85257D-06	1	16.5781	12	3.85257D-06
13	3.96137E-06	3.75700D-06	1	18.0852	13	3.75700D-06
14	3.85343E-06	3.65463D-06	1	19.5923	14	3.65463D-06
15	3.73870E-06	3.54582D-06	1	21.0994	15	3.54582D-06
16	3.61755E-06	3.43092D-06	1	22.6065	16	3.43092D-06
17	3.49039E-06	3.31032D-06	1	24.1136	17	3.31032D-06
18	3.35761E-06	3.18439D-06	1	25.6207	18	3.18439D-06
19	3.21964E-06	3.05354D-06	1	27.1278	19	3.05354D-06
20	3.07689E-06	2.91815D-06	1	28.6349	20	2.91815D-06
21	2.92977E-06	2.77862D-06	1	30.1420	21	2.77862D-06
22	2.77871E-06	2.63536D-06	1	31.6491	22	2.63536D-06
23	2.62413E-06	2.48875D-06	1	33.1562	23	2.48875D-06
24	2.46641E-06	2.33917D-06	1	34.6633	24	2.33917D-06
25	2.30597E-06	2.18701D-06	1	36.1704	25	2.18701D-06
26	2.14319E-06	2.03262D-06	1	37.6775	26	2.03262D-06
27	1.97843E-06	1.87636D-06	1	39.1846	27	1.87636D-06
28	1.81204E-06	1.71856D-06	1	40.6917	28	1.71856D-06
29	1.72838E-06	1.63921D-06	1	41.4452		
30	1.64442E-06	1.55959D-06	1	42.1988	29	1.55959D-06
31	1.60235E-06	1.51968D-06	1	42.5756		
32	1.56021E-06	1.47972D-06	1	42.9523		
33	1.51801E-06	1.43970D-06	1	43.3291		
34	1.47575E-06	1.39961D-06	1	43.7059	30	1.39961D-06
35	1.45460E-06	1.37955D-06	1	43.8943		
36	1.43343E-06	1.35948D-06	1	44.0827		
37	1.41224E-06	1.33939D-06	1	44.2710		
38	1.39104E-06	1.31928D-06	1	44.4594		
39	1.36983E-06	1.29916D-06	1	44.6478		
40	1.34860E-06	1.27902D-06	1	44.8362		
41	1.32735E-06	1.25887D-06	1	45.0246		
42	1.30609E-06	1.23871D-06	1	45.2130	31	1.23871D-06
43	6.54057E-07	6.20314D-07	2	45.2130	32	6.20314D-07
44	5.46251E-07	5.18069D-07	2	45.9630		
45	4.56758E-07	4.33193D-07	2	46.7130	33	4.33193D-07
46	3.22595E-07	3.05953D-07	2	48.2130	34	3.05953D-07
47	2.29554E-07	2.17711D-07	2	49.7130	35	2.17711D-07
48	1.64666E-07	1.56171D-07	2	51.2130	36	1.56171D-07
49	1.19133E-07	1.12987D-07	2	52.7130	37	1.12987D-07
50	8.69649E-08	8.24783D-08	2	54.2130	38	8.24783D-08
51	6.40687E-08	6.07634D-08	2	55.7130	39	6.07634D-08
52	4.76385E-08	4.51808D-08	2	57.2130	40	4.51808D-08
53	3.57424E-08	3.38984D-08	2	58.7130	41	3.38984D-08
54	2.70449E-08	2.56496D-08	2	60.2130	42	2.56496D-08
55	2.06184E-08	1.95546D-08	2	61.7130	43	1.95546D-08
56	1.58153E-08	1.49993D-08	2	63.2130	44	1.49993D-08
57	1.21808E-08	1.15524D-08	2	64.7130	45	1.15524D-08
58	9.39357E-09	8.90895D-09	2	66.2130	46	8.90895D-09
59	7.22476E-09	6.85203D-09	2	67.7130	47	6.85203D-09
60	5.51012E-09	5.22585D-09	2	69.2130	48	5.22585D-09
61	4.13073E-09	3.91763D-09	2	70.7130	49	3.91763D-09
62	2.99971E-09	2.84495D-09	2	72.2130	50	2.84495D-09
63	2.05298E-09	1.94707D-09	2	73.7130	51	1.94707D-09
64	1.24303E-09	1.17891D-09	2	75.2130	52	1.17891D-09

NEUTRON FLUX PRODUCED BY (1/K) * FISSION SOURCE WHERE NORM OF F.S. = 1

POINT	RADIUS	GROUP 1	2	3	4	5	6	7	8	9	10
1	0.0	1.2568E-08	1.6995E-08	2.1598E-08	2.6330E-08	3.4032E-08	4.2067E-08	5.0531E-08	5.5854E-08	6.4681E-08	8.1309E-08
2	1.5071	1.2555E-08	1.6978E-08	2.1575E-08	2.6802E-08	3.3997E-08	4.2023E-08	5.0478E-08	5.5796E-08	6.4614E-08	8.1224E-08
3	3.0142	1.2516E-08	1.6924E-08	2.1507E-08	2.6718E-08	3.3890E-08	4.1890E-08	5.0320E-08	5.5621E-08	6.4412E-08	8.0970E-08
4	4.5213	1.2450E-08	1.6836E-08	2.1395E-08	2.6578E-08	3.3712E-08	4.1671E-08	5.0056E-08	5.5330E-08	6.4076E-08	8.0547E-08
5	6.0284	1.2359E-08	1.6712E-08	2.1237E-08	2.6382E-08	3.3464E-08	4.1364E-08	4.9687E-08	5.4925E-08	6.3607E-08	7.9957E-08
6	7.5355	1.2242E-08	1.6553E-08	2.1036E-08	2.6132E-08	3.3146E-08	4.0971E-08	4.9215E-08	5.4406E-08	6.3007E-08	7.9201E-08
7	9.0426	1.2100E-08	1.6361E-08	2.0791E-08	2.5828E-08	3.2760E-08	4.0493E-08	4.8642E-08	5.3775E-08	6.2278E-08	7.8283E-08
8	10.5497	1.1933E-08	1.6135E-08	2.0504E-08	2.5471E-08	3.2306E-08	3.9932E-08	4.7969E-08	5.3034E-08	6.1422E-08	7.7205E-08
9	12.0568	1.1742E-08	1.5876E-08	2.0174E-08	2.5062E-08	3.1787E-08	3.9290E-08	4.7198E-08	5.2186E-08	6.0441E-08	7.5970E-08
10	13.5639	1.1527E-08	1.5584E-08	1.9804E-08	2.4603E-08	3.1203E-08	3.8568E-08	4.6331E-08	5.1232E-08	5.9340E-08	7.4582E-08
11	15.0710	1.1289E-08	1.5262E-08	1.9395E-08	2.4094E-08	3.0557E-08	3.7768E-08	4.5372E-08	5.0177E-08	5.8120E-08	7.3045E-08
12	16.5781	1.1029E-08	1.4910E-08	1.8947E-08	2.3537E-08	2.9850E-08	3.6894E-08	4.4322E-08	4.9023E-08	5.6786E-08	7.1365E-08
13	18.0852	1.0747E-08	1.4528E-08	1.8461E-08	2.2935E-08	2.9084E-08	3.5947E-08	4.3186E-08	4.7773E-08	5.5342E-08	6.9545E-08
14	19.5923	1.0445E-08	1.4118E-08	1.7940E-08	2.2288E-08	2.8262E-08	3.4931E-08	4.1965E-08	4.6431E-08	5.3792E-08	6.7591E-08
15	21.0994	1.0123E-08	1.3682E-08	1.7385E-08	2.1598E-08	2.7386E-08	3.3847E-08	4.0665E-08	4.5000E-08	5.2139E-08	6.5508E-08
16	22.6065	9.7816E-09	1.3219E-08	1.6797E-08	2.0867E-08	2.6458E-08	3.2699E-08	3.9287E-08	4.3485E-08	5.0388E-08	6.3301E-08
17	24.1136	9.4221E-09	1.2732E-08	1.6177E-08	2.0097E-08	2.5480E-08	3.1490E-08	3.7835E-08	4.1888E-08	4.8543E-08	6.0975E-08
18	25.6207	9.0452E-09	1.2221E-08	1.5527E-08	1.9290E-08	2.4455E-08	3.0222E-08	3.6313E-08	4.0214E-08	4.6608E-08	5.8537E-08
19	27.1278	8.6518E-09	1.1688E-08	1.4849E-08	1.8447E-08	2.3384E-08	2.8899E-08	3.4724E-08	3.8465E-08	4.4587E-08	5.5989E-08
20	28.6349	8.2426E-09	1.1133E-08	1.4144E-08	1.7570E-08	2.2271E-08	2.7522E-08	3.3071E-08	3.6645E-08	4.2484E-08	5.3337E-08
21	30.1420	7.8184E-09	1.0558E-08	1.3412E-08	1.6661E-08	2.1116E-08	2.6095E-08	3.1358E-08	3.4757E-08	4.0300E-08	5.0586E-08
22	31.6491	7.3797E-09	9.9636E-09	1.2656E-08	1.5721E-08	1.9922E-08	2.4620E-08	2.9587E-08	3.2802E-08	3.8039E-08	4.7737E-08
23	33.1562	6.9273E-09	9.3507E-09	1.1875E-08	1.4751E-08	1.8691E-08	2.3099E-08	2.7759E-08	3.0784E-08	3.5703E-08	4.4795E-08
24	34.6633	6.4615E-09	8.7199E-09	1.1072E-08	1.3752E-08	1.7424E-08	2.1534E-08	2.5879E-08	2.8702E-08	3.3291E-08	4.1760E-08
25	36.1704	5.9826E-09	8.0717E-09	1.0247E-08	1.2725E-08	1.6122E-08	1.9926E-08	2.3946E-08	2.6557E-08	3.0803E-08	3.8633E-08
26	37.6775	5.4907E-09	7.4065E-09	9.3993E-09	1.1669E-08	1.4785E-08	1.8277E-08	2.1962E-08	2.4347E-08	2.8236E-08	3.5412E-08
27	39.1846	4.9857E-09	6.7242E-09	8.5295E-09	1.0586E-08	1.3414E-08	1.6586E-08	1.9927E-08	2.2070E-08	2.5586E-08	3.2093E-08
28	40.6917	4.4673E-09	6.0246E-09	7.6372E-09	9.4732E-09	1.2008E-08	1.4854E-08	1.7840E-08	1.9722E-08	2.2846E-08	2.8672E-08
29	42.1988	3.9345E-09	5.3070E-09	6.7212E-09	8.3300E-09	1.0566E-08	1.3078E-08	1.5699E-08	1.7295E-08	2.0004E-08	2.5136E-08
30	43.7059	3.3864E-09	4.5703E-09	5.7799E-09	7.1538E-09	9.0851E-09	1.1257E-08	1.3500E-08	1.4778E-08	1.7046E-08	2.1475E-08
31	45.2130	2.8214E-09	3.8128E-09	4.8112E-09	5.9416E-09	7.5629E-09	9.3876E-09	1.1239E-08	1.2161E-08	1.3953E-08	1.7672E-08
32	45.2130	2.8214E-09	3.8128E-09	4.8112E-09	5.9416E-09	7.5629E-09	9.3876E-09	1.1239E-08	1.2161E-08	1.3953E-08	1.7672E-08
33	46.7130	1.9579E-09	2.6475E-09	3.3372E-09	4.1196E-09	5.2241E-09	6.4772E-09	7.7667E-09	8.4909E-09	9.7771E-09	1.2329E-08
34	48.2130	1.3678E-09	1.8505E-09	2.3304E-09	2.8756E-09	3.6346E-09	4.5016E-09	5.4051E-09	5.9638E-09	6.8897E-09	8.6543E-09
35	49.7130	9.5849E-10	1.2971E-09	1.6321E-09	2.0133E-09	2.5369E-09	3.1388E-09	3.7736E-09	4.1994E-09	4.8664E-09	6.0914E-09
36	51.2130	6.7397E-10	9.1225E-10	1.1469E-09	1.4144E-09	1.7771E-09	2.1967E-09	2.6440E-09	2.9659E-09	3.4472E-09	4.3009E-09
37	52.7130	4.7578E-10	6.4401E-10	8.0912E-10	9.9760E-10	1.2501E-09	1.5438E-09	1.8602E-09	2.1022E-09	2.4502E-09	3.0479E-09
38	54.2130	3.3739E-10	4.5661E-10	5.7330E-10	7.0672E-10	8.8338E-10	1.0900E-09	1.3147E-09	1.4962E-09	1.7486E-09	2.1690E-09
39	55.7130	2.4045E-10	3.2531E-10	4.0820E-10	5.0314E-10	6.2747E-10	7.7357E-10	9.3398E-10	1.0698E-09	1.2535E-09	1.5508E-09
40	57.2130	1.7231E-10	2.3300E-10	2.9222E-10	3.6016E-10	4.4822E-10	5.5214E-10	6.6723E-10	7.6894E-10	9.0316E-10	1.1146E-09
41	58.7130	1.2422E-10	1.6784E-10	2.1041E-10	2.5933E-10	3.2212E-10	3.9650E-10	4.7956E-10	5.5580E-10	6.5433E-10	8.0568E-10
42	60.2130	9.0112E-11	1.2165E-10	1.5244E-10	1.8789E-10	2.3298E-10	2.8658E-10	3.4688E-10	4.0414E-10	4.7683E-10	5.8585E-10
43	61.7130	6.5790E-11	8.8719E-11	1.1114E-10	1.3700E-10	1.6961E-10	2.0849E-10	2.5255E-10	2.9565E-10	3.4955E-10	4.2860E-10
44	63.2130	4.8333E-11	6.5099E-11	8.1528E-11	1.0051E-10	1.2426E-10	1.5266E-10	1.8504E-10	2.1758E-10	2.5773E-10	3.1542E-10
45	64.7130	3.5712E-11	4.8037E-11	6.0146E-11	7.4161E-11	9.1577E-11	1.1245E-10	1.3637E-10	1.6099E-10	1.9103E-10	2.3338E-10
46	66.2130	2.6511E-11	3.5613E-11	4.4581E-11	5.4979E-11	6.7819E-11	8.3233E-11	1.0099E-10	1.1964E-10	1.4219E-10	1.7343E-10
47	67.7130	1.9743E-11	2.6487E-11	3.3151E-11	4.0889E-11	5.0392E-11	6.1816E-11	7.5036E-11	8.9159E-11	1.0610E-10	1.2923E-10
48	69.2130	1.4719E-11	1.9723E-11	2.4680E-11	3.0444E-11	3.7487E-11	4.5964E-11	5.5809E-11	6.6479E-11	7.9198E-11	9.6327E-11
49	70.7130	1.0957E-11	1.4668E-11	1.8349E-11	2.2633E-11	2.7847E-11	3.4126E-11	4.1437E-11	4.9454E-11	5.8957E-11	7.1617E-11
50	72.2130	8.1262E-12	1.0869E-11	1.3591E-11	1.6760E-11	2.0601E-11	2.5229E-11	3.0626E-11	3.6593E-11	4.3631E-11	5.2929E-11
51	73.7130	6.0012E-12	8.0214E-12	1.0023E-11	1.2350E-11	1.5162E-11	1.8548E-11	2.2496E-11	2.6880E-11	3.2025E-11	3.8783E-11
52	75.2130	4.4394E-12	5.9279E-12	7.3969E-12	9.1012E-12	1.1153E-11	1.3618E-11	1.6482E-11	1.9658E-11	2.3361E-11	2.8213E-11

POINT	RADIUS	GROUP 11	12	13	14	15	16	17	18	19	20
1	0.0	9.9009E-08	1.3140E-07	1.5153E-07	1.7496E-07	1.8723E-07	2.0778E-07	2.5117E-07	2.8543E-07	3.1635E-07	3.3729E-07
2	1.5071	9.8906E-08	1.3126E-07	1.5137E-07	1.7478E-07	1.8704E-07	2.0757E-07	2.5091E-07	2.8513E-07	3.1601E-07	3.3693E-07

3	3.0142	9.8596E-08	1.3085E-07	1.5090E-07	1.7423E-07	1.8645E-07	2.0692E-07	2.5012E-07	2.8423E-07	3.1502E-07	3.3588E-07
4	4.5213	9.8080E-08	1.3016E-07	1.5010E-07	1.7331E-07	1.8547E-07	2.0583E-07	2.4881E-07	2.8274E-07	3.1337E-07	3.3412E-07
5	6.0284	9.7361E-08	1.2920E-07	1.4900E-07	1.7204E-07	1.8411E-07	2.0433E-07	2.4699E-07	2.8067E-07	3.1107E-07	3.3167E-07
6	7.5355	9.6440E-08	1.2797E-07	1.4758E-07	1.7040E-07	1.8237E-07	2.0240E-07	2.4465E-07	2.7801E-07	3.0812E-07	3.2853E-07
7	9.0426	9.5320E-08	1.2648E-07	1.4586E-07	1.6842E-07	1.8025E-07	2.0005E-07	2.4180E-07	2.7477E-07	3.0454E-07	3.2471E-07
8	10.5497	9.4005E-08	1.2472E-07	1.4384E-07	1.6608E-07	1.7777E-07	1.9729E-07	2.3846E-07	2.7098E-07	3.0033E-07	3.2023E-07
9	12.0568	9.2499E-08	1.2271E-07	1.4152E-07	1.6341E-07	1.7492E-07	1.9414E-07	2.3464E-07	2.6663E-07	2.9552E-07	3.1510E-07
10	13.5639	9.0807E-08	1.2046E-07	1.3892E-07	1.6041E-07	1.7172E-07	1.9059E-07	2.3034E-07	2.6174E-07	2.9010E-07	3.0934E-07
11	15.0710	8.8934E-08	1.1796E-07	1.3604E-07	1.5709E-07	1.6818E-07	1.8667E-07	2.2559E-07	2.5633E-07	2.8411E-07	3.0296E-07
12	16.5781	8.6885E-08	1.1522E-07	1.3289E-07	1.5345E-07	1.6431E-07	1.8238E-07	2.2039E-07	2.5042E-07	2.7756E-07	2.9598E-07
13	18.0852	8.4666E-08	1.1226E-07	1.2948E-07	1.4952E-07	1.6011E-07	1.7773E-07	2.1475E-07	2.4402E-07	2.7046E-07	2.8843E-07
14	19.5923	8.2283E-08	1.0908E-07	1.2582E-07	1.4530E-07	1.5561E-07	1.7275E-07	2.0871E-07	2.3714E-07	2.6284E-07	2.8032E-07
15	21.0994	7.9743E-08	1.0569E-07	1.2192E-07	1.4080E-07	1.5082E-07	1.6743E-07	2.0226E-07	2.2982E-07	2.5473E-07	2.7167E-07
16	22.6065	7.7052E-08	1.0210E-07	1.1779E-07	1.3604E-07	1.4574E-07	1.6181E-07	1.9544E-07	2.2206E-07	2.4613E-07	2.6252E-07
17	24.1136	7.4217E-08	9.8323E-08	1.1344E-07	1.3102E-07	1.4039E-07	1.5588E-07	1.8826E-07	2.1389E-07	2.3707E-07	2.5288E-07
18	25.6207	7.1244E-08	9.4362E-08	1.0889E-07	1.2577E-07	1.3479E-07	1.4967E-07	1.8073E-07	2.0533E-07	2.2759E-07	2.4279E-07
19	27.1278	6.8139E-08	9.0229E-08	1.0413E-07	1.2029E-07	1.2894E-07	1.4319E-07	1.7287E-07	1.9639E-07	2.1768E-07	2.3225E-07
20	28.6349	6.4907E-08	8.5932E-08	9.9196E-08	1.1460E-07	1.2287E-07	1.3645E-07	1.6470E-07	1.8710E-07	2.0739E-07	2.2129E-07
21	30.1420	6.1555E-08	8.1482E-08	9.4085E-08	1.0871E-07	1.1657E-07	1.2946E-07	1.5624E-07	1.7748E-07	1.9673E-07	2.0994E-07
22	31.6491	5.8087E-08	7.6887E-08	8.8809E-08	1.0263E-07	1.1007E-07	1.2224E-07	1.4750E-07	1.6755E-07	1.8571E-07	1.9821E-07
23	33.1562	5.4506E-08	7.2154E-08	8.3380E-08	9.6371E-08	1.0337E-07	1.1480E-07	1.3850E-07	1.5731E-07	1.7435E-07	1.8613E-07
24	34.6633	5.0815E-08	6.7292E-08	7.7806E-08	8.9950E-08	9.6485E-08	1.0714E-07	1.2924E-07	1.4678E-07	1.6267E-07	1.7370E-07
25	36.1704	4.7016E-08	6.2307E-08	7.2096E-08	8.3375E-08	8.9414E-08	9.9270E-08	1.1974E-07	1.3598E-07	1.5069E-07	1.6095E-07
26	37.6775	4.3107E-08	5.7206E-08	6.6259E-08	7.6653E-08	8.2166E-08	9.1188E-08	1.1001E-07	1.2491E-07	1.3840E-07	1.4787E-07
27	39.1846	3.9087E-08	5.1994E-08	6.0299E-08	6.9794E-08	7.4741E-08	8.2894E-08	1.0004E-07	1.1358E-07	1.2581E-07	1.3446E-07
28	40.6917	3.4950E-08	4.6674E-08	5.4224E-08	6.2802E-08	6.7138E-08	7.4382E-08	8.9853E-08	1.0200E-07	1.1293E-07	1.2074E-07
29	42.1988	3.0687E-08	4.1250E-08	4.8037E-08	5.5685E-08	5.9350E-08	6.5637E-08	7.9431E-08	9.0144E-08	9.9732E-08	1.0668E-07
30	43.7059	2.6287E-08	3.5724E-08	4.1740E-08	4.8442E-08	5.1367E-08	5.6640E-08	6.8769E-08	7.8018E-08	8.6216E-08	9.2268E-08
31	45.2130	2.1734E-08	3.0094E-08	3.5334E-08	4.1076E-08	4.3171E-08	4.7364E-08	5.7855E-08	6.5602E-08	7.2353E-08	7.7473E-08
32	45.2130	2.1734E-08	3.0094E-08	3.5334E-08	4.1076E-08	4.3171E-08	4.7364E-08	5.7855E-08	6.5602E-08	7.2353E-08	7.7473E-08
33	46.7130	1.5181E-08	2.0950E-08	2.4886E-08	2.9086E-08	3.0917E-08	3.3962E-08	4.1073E-08	4.6470E-08	5.1171E-08	5.4830E-08
34	48.2130	1.0666E-08	1.4675E-08	1.7613E-08	2.0686E-08	2.2209E-08	2.4426E-08	2.9285E-08	3.3064E-08	3.6357E-08	3.8979E-08
35	49.7130	7.5134E-09	1.0306E-08	1.2486E-08	1.4733E-08	1.5964E-08	1.7579E-08	2.0911E-08	2.3562E-08	2.5873E-08	2.7754E-08
36	51.2130	5.3092E-09	7.2594E-09	8.8710E-09	1.0512E-08	1.1488E-08	1.2666E-08	1.4959E-08	1.6823E-08	1.8451E-08	1.9801E-08
37	52.7130	3.7634E-09	5.1310E-09	6.3190E-09	7.5185E-09	8.2815E-09	9.1427E-09	1.0728E-08	1.2042E-08	1.3192E-08	1.4164E-08
38	54.2130	2.6788E-09	3.6408E-09	4.5151E-09	5.3924E-09	5.9836E-09	6.6146E-09	7.7152E-09	8.6448E-09	9.4608E-09	1.0163E-08
39	55.7130	1.9155E-09	2.5947E-09	3.2379E-09	3.8803E-09	4.3353E-09	4.7992E-09	5.5673E-09	6.2276E-09	6.8093E-09	7.3180E-09
40	57.2130	1.3766E-09	1.8583E-09	2.3314E-09	2.8027E-09	3.1515E-09	3.4936E-09	4.0327E-09	4.5039E-09	4.9208E-09	5.2911E-09
41	58.7130	9.9477E-10	1.3379E-09	1.6863E-09	2.0328E-09	2.2994E-09	2.5528E-09	2.9335E-09	3.2714E-09	3.5719E-09	3.8429E-09
42	60.2130	7.2302E-10	9.6865E-10	1.2257E-09	1.4811E-09	1.6846E-09	1.8729E-09	2.1435E-09	2.3873E-09	2.6052E-09	2.8046E-09
43	61.7130	5.2864E-10	7.0539E-10	8.9532E-10	1.0842E-09	1.2394E-09	1.3800E-09	1.5736E-09	1.7504E-09	1.9095E-09	2.0570E-09
44	63.2130	3.8876E-10	5.1660E-10	6.5728E-10	7.9730E-10	9.1565E-10	1.0210E-09	1.1605E-09	1.2855E-09	1.4063E-09	1.5160E-09
45	64.7130	2.8740E-10	3.8034E-10	4.8476E-10	5.8884E-10	6.7907E-10	7.5831E-10	8.5944E-10	9.5403E-10	1.0403E-09	1.1222E-09
46	66.2130	2.1338E-10	2.8123E-10	3.5838E-10	4.3639E-10	5.0512E-10	5.6482E-10	6.3854E-10	7.0820E-10	7.7213E-10	8.3354E-10
47	67.7130	1.5885E-10	2.0855E-10	2.6632E-10	3.2410E-10	3.7635E-10	4.2133E-10	4.7526E-10	5.2669E-10	5.7417E-10	6.2022E-10
48	69.2130	1.1830E-10	1.5476E-10	1.9771E-10	2.4072E-10	2.8027E-10	3.1408E-10	3.5357E-10	3.9151E-10	4.2673E-10	4.6118E-10
49	70.7130	8.7869E-11	1.1460E-10	1.4641E-10	1.7831E-10	2.0802E-10	2.3325E-10	2.6207E-10	2.8993E-10	3.1589E-10	3.4145E-10
50	72.2130	6.4870E-11	8.4377E-11	1.0778E-10	1.3124E-10	1.5329E-10	1.7187E-10	1.9272E-10	2.1294E-10	2.3181E-10	2.5048E-10
51	73.7130	4.7458E-11	6.1583E-11	7.8600E-11	9.5612E-11	1.1165E-10	1.2504E-10	1.3986E-10	1.5424E-10	1.6760E-10	1.8087E-10
52	75.2130	3.4422E-11	4.4534E-11	5.6684E-11	6.8756E-11	8.0073E-11	8.9384E-11	9.9606E-11	1.0948E-10	1.1855E-10	1.2755E-10

POINT	GROUP / RADIUS	21	22	23	24	25	26	27	28	29	30
1	0.0	3.9147E-07	4.3409E-07	4.6380E-07	4.9675E-07	5.2892E-07	5.3969E-07	5.9803E-07	6.5359E-07	6.4291E-07	6.6031E-07
2	1.5071	3.9106E-07	4.3363E-07	4.6332E-07	4.9623E-07	5.2836E-07	5.3912E-07	5.9740E-07	6.5291E-07	6.4224E-07	6.5962E-07
3	3.0142	3.8984E-07	4.3227E-07	4.6186E-07	4.9467E-07	5.2671E-07	5.3744E-07	5.9554E-07	6.5087E-07	6.4023E-07	6.5756E-07
4	4.5213	3.8779E-07	4.3000E-07	4.5944E-07	4.9208E-07	5.2395E-07	5.3463E-07	5.9243E-07	6.4747E-07	6.3689E-07	6.5413E-07
5	6.0284	3.8494E-07	4.2684E-07	4.5606E-07	4.8846E-07	5.2010E-07	5.3071E-07	5.8809E-07	6.4273E-07	6.3222E-07	6.4934E-07
6	7.5355	3.8129E-07	4.2279E-07	4.5174E-07	4.8383E-07	5.1518E-07	5.2570E-07	5.8253E-07	6.3665E-07	6.2626E-07	6.4322E-07
7	9.0426	3.7685E-07	4.1786E-07	4.4648E-07	4.7821E-07	5.0919E-07	5.1961E-07	5.7578E-07	6.2928E-07	6.1900E-07	6.3578E-07
8	10.5497	3.7164E-07	4.1208E-07	4.4031E-07	4.7160E-07	5.0217E-07	5.1245E-07	5.6785E-07	6.2061E-07	6.1048E-07	6.2703E-07
9	12.0568	3.6567E-07	4.0546E-07	4.3324E-07	4.6404E-07	4.9412E-07	5.0426E-07	5.5878E-07	6.1069E-07	6.0073E-07	6.1703E-07
10	13.5639	3.5897E-07	3.9802E-07	4.2530E-07	4.5553E-07	4.8508E-07	4.9506E-07	5.4858E-07	5.9954E-07	5.8977E-07	6.0578E-07
11	15.0710	3.5154E-07	3.8979E-07	4.1651E-07	4.4612E-07	4.7507E-07	4.8487E-07	5.3728E-07	5.8720E-07	5.7764E-07	5.9333E-07
12	16.5781	3.4343E-07	3.8078E-07	4.0689E-07	4.3583E-07	4.6412E-07	4.7372E-07	5.2493E-07	5.7370E-07	5.6436E-07	5.7971E-07
13	18.0852	3.3464E-07	3.7104E-07	3.9648E-07	4.2469E-07	4.5227E-07	4.6166E-07	5.1156E-07	5.5908E-07	5.4999E-07	5.6497E-07

NEUTRON CURRENT

POINT	GROUP / RADIUS	1	2	3	4	5	6	7	8	9	10
1	0.0	0.0	0.0	0.0	0.0	0.0	0.0	0.0	0.0	0.0	0.0
2	1.5071	7.5040E-11	1.0188E-10	1.2735E-10	1.5512E-10	2.0057E-10	2.4962E-10	2.9222E-10	2.8699E-10	3.1393E-10	4.0909E-10
3	3.0142	1.4983E-10	2.0341E-10	2.5427E-10	3.0972E-10	4.0047E-10	4.9843E-10	5.8346E-10	5.7301E-10	6.2680E-10	8.1680E-10
4	4.5213	2.2413E-10	3.0429E-10	3.8037E-10	4.6332E-10	5.9908E-10	7.4562E-10	8.7282E-10	8.5715E-10	9.3761E-10	1.2219E-09
5	6.0284	2.9770E-10	4.0418E-10	5.0524E-10	6.1542E-10	7.9577E-10	9.9041E-10	1.1594E-09	1.1385E-09	1.2453E-09	1.6229E-09
6	7.5355	3.7030E-10	5.0278E-10	6.2849E-10	7.6556E-10	9.8992E-10	1.2320E-09	1.4422E-09	1.4162E-09	1.5490E-09	2.0188E-09
7	9.0426	4.4173E-10	5.9978E-10	7.4975E-10	9.1326E-10	1.1809E-09	1.4698E-09	1.7205E-09	1.6893E-09	1.8477E-09	2.4082E-09
8	10.5497	5.1175E-10	6.9488E-10	8.6865E-10	1.0581E-09	1.3683E-09	1.7029E-09	1.9934E-09	1.9571E-09	2.1405E-09	2.7900E-09
9	12.0568	5.8018E-10	7.8783E-10	9.8486E-10	1.1997E-09	1.5513E-09	1.9308E-09	2.2601E-09	2.2188E-09	2.4266E-09	3.1632E-09
10	13.5639	6.4682E-10	8.7838E-10	1.0981E-09	1.3376E-09	1.7297E-09	2.1528E-09	2.5200E-09	2.4737E-09	2.7053E-09	3.5267E-09
11	15.0710	7.1152E-10	9.6629E-10	1.2080E-09	1.4715E-09	1.9030E-09	2.3684E-09	2.7723E-09	2.7212E-09	2.9758E-09	3.8797E-09
12	16.5781	7.7412E-10	1.0514E-09	1.3144E-09	1.6012E-09	2.0707E-09	2.5771E-09	3.0166E-09	2.9607E-09	3.2376E-09	4.2215E-09
13	18.0852	8.3452E-10	1.1335E-09	1.4171E-09	1.7263E-09	2.2325E-09	2.7785E-09	3.2524E-09	3.1919E-09	3.4903E-09	4.5514E-09
14	19.5923	8.9260E-10	1.2124E-09	1.5159E-09	1.8467E-09	2.3883E-09	2.9723E-09	3.4791E-09	3.4144E-09	3.7335E-09	4.8690E-09
15	21.0994	9.4831E-10	1.2881E-09	1.6107E-09	1.9622E-09	2.5377E-09	3.1581E-09	3.6967E-09	3.6280E-09	3.9670E-09	5.1741E-09
16	22.6065	1.0016E-09	1.3606E-09	1.7014E-09	2.0728E-09	2.6807E-09	3.3359E-09	3.9049E-09	3.8327E-09	4.1909E-09	5.4665E-09
17	24.1136	1.0525E-09	1.4297E-09	1.7880E-09	2.1785E-09	2.8173E-09	3.5056E-09	4.1038E-09	4.0285E-09	4.4053E-09	5.7464E-09
18	25.6207	1.1010E-09	1.4956E-09	1.8705E-09	2.2793E-09	2.9474E-09	3.6673E-09	4.2933E-09	4.2158E-09	4.6106E-09	6.0143E-09
19	27.1278	1.1472E-09	1.5583E-09	1.9492E-09	2.3755E-09	3.0715E-09	3.8212E-09	4.4738E-09	4.3951E-09	4.8074E-09	6.2708E-09
20	28.6349	1.1912E-09	1.6180E-09	2.0241E-09	2.4672E-09	3.1896E-09	3.9676E-09	4.6457E-09	4.5669E-09	4.9967E-09	6.5170E-09
21	30.1420	1.2333E-09	1.6749E-09	2.0957E-09	2.5549E-09	3.3022E-09	4.1069E-09	4.8096E-09	4.7325E-09	5.1799E-09	6.7541E-09
22	31.6491	1.2736E-09	1.7292E-09	2.1641E-09	2.6390E-09	3.4099E-09	4.2399E-09	4.9663E-09	4.8930E-09	5.3585E-09	6.9842E-09
23	33.1562	1.3125E-09	1.7814E-09	2.2300E-09	2.7201E-09	3.5134E-09	4.3673E-09	5.1170E-09	5.0502E-09	5.5347E-09	7.2094E-09
24	34.6633	1.3503E-09	1.8319E-09	2.2939E-09	2.7991E-09	3.6136E-09	4.4902E-09	5.2628E-09	5.2062E-09	5.7114E-09	7.4326E-09
25	36.1704	1.3876E-09	1.8813E-09	2.3566E-09	2.8770E-09	3.7115E-09	4.6098E-09	5.4054E-09	5.3636E-09	5.8920E-09	7.6576E-09
26	37.6775	1.4249E-09	1.9302E-09	2.4190E-09	2.9548E-09	3.8084E-09	4.7276E-09	5.5468E-09	5.5258E-09	6.0808E-09	7.8885E-09
27	39.1846	1.4629E-09	1.9794E-09	2.4820E-09	3.0340E-09	3.9060E-09	4.8454E-09	5.6893E-09	5.6967E-09	6.2832E-09	8.1309E-09
28	40.6917	1.5025E-09	2.0300E-09	2.5471E-09	3.1163E-09	4.0061E-09	4.9654E-09	5.8357E-09	5.8815E-09	6.5059E-09	8.3912E-09
29	42.1988	1.5447E-09	2.0830E-09	2.6156E-09	3.2036E-09	4.1107E-09	5.0899E-09	5.9891E-09	6.0858E-09	6.7565E-09	8.6766E-09
30	43.7059	1.5906E-09	2.1398E-09	2.6895E-09	3.2983E-09	4.2226E-09	5.2220E-09	6.1536E-09	6.3176E-09	7.0460E-09	8.9973E-09
31	45.2130	1.6418E-09	2.2021E-09	2.7708E-09	3.4034E-09	4.3447E-09	5.3650E-09	6.3337E-09	6.5860E-09	7.3871E-09	9.3647E-09
32	45.2130	1.6418E-09	2.2021E-09	2.7708E-09	3.4034E-09	4.3447E-09	5.3650E-09	6.3337E-09	6.5860E-09	7.3871E-09	9.3647E-09
33	46.7130	1.1381E-09	1.5279E-09	1.9201E-09	2.3573E-09	2.9966E-09	3.6958E-09	4.3707E-09	4.5992E-09	5.1794E-09	6.5311E-09
34	48.2130	7.8900E-10	1.0601E-09	1.3306E-09	1.6328E-09	2.0674E-09	2.5469E-09	3.0168E-09	3.2099E-09	3.6285E-09	4.5533E-09
35	49.7130	5.4786E-10	7.3662E-10	9.2366E-10	1.1329E-09	1.4292E-09	1.7587E-09	2.0863E-09	2.2425E-09	2.5439E-09	3.1784E-09
36	51.2130	3.8117E-10	5.1282E-10	6.4240E-10	7.8762E-10	9.9021E-10	1.2172E-09	1.4459E-09	1.5689E-09	1.7857E-09	2.2223E-09
37	52.7130	2.6581E-10	3.5780E-10	4.4781E-10	5.4884E-10	6.8782E-10	8.4463E-10	1.0046E-09	1.0996E-09	1.2555E-09	1.5568E-09
38	54.2130	1.8587E-10	2.5030E-10	3.1300E-10	3.8349E-10	4.7918E-10	5.8786E-10	7.0006E-10	7.7250E-10	8.8462E-10	1.0933E-09
39	55.7130	1.3039E-10	1.7563E-10	2.1947E-10	2.6881E-10	3.3497E-10	4.1055E-10	4.8946E-10	5.4422E-10	6.2497E-10	7.7008E-10
40	57.2130	9.1818E-11	1.2369E-10	1.5445E-10	1.8913E-10	2.3507E-10	2.8785E-10	3.4354E-10	3.8470E-10	4.4298E-10	5.4429E-10
41	58.7130	6.4940E-11	8.7472E-11	1.0916E-10	1.3365E-10	1.6571E-10	2.0275E-10	2.4221E-10	2.7304E-10	3.1523E-10	3.8629E-10
42	60.2130	4.6165E-11	6.2165E-11	7.7534E-11	9.4915E-11	1.1743E-10	1.4356E-10	1.7166E-10	1.9473E-10	2.2538E-10	2.7550E-10
43	61.7130	3.3014E-11	4.4433E-11	5.5390E-11	6.7803E-11	8.3716E-11	1.0226E-10	1.2239E-10	1.3966E-10	1.6203E-10	1.9759E-10
44	63.2130	2.3770E-11	3.1968E-11	3.9834E-11	4.8761E-11	6.0093E-11	7.3352E-11	8.7861E-11	1.0082E-10	1.1724E-10	1.4265E-10
45	64.7130	1.7247E-11	2.3172E-11	2.8864E-11	3.5335E-11	4.3473E-11	5.3030E-11	6.3570E-11	7.3331E-11	8.5467E-11	1.0377E-10
46	66.2130	1.2622E-11	1.6937E-11	2.1091E-11	2.5824E-11	3.1724E-11	3.8674E-11	4.6397E-11	5.3786E-11	6.2825E-11	7.6122E-11
47	67.7130	9.3216E-12	1.2490E-11	1.5550E-11	1.9045E-11	2.3366E-11	2.8471E-11	3.4182E-11	3.9811E-11	4.6601E-11	5.6356E-11
48	69.2130	6.9459E-12	9.2914E-12	1.1567E-11	1.4172E-11	1.7370E-11	2.1155E-11	2.5420E-11	2.9737E-11	3.4883E-11	4.2112E-11
49	70.7130	5.2124E-12	6.9606E-12	8.6662E-12	1.0624E-11	1.3010E-11	1.5843E-11	1.9054E-11	2.2385E-11	2.6317E-11	3.1726E-11
50	72.2130	3.9185E-12	5.2252E-12	6.5074E-12	7.9837E-12	9.7731E-12	1.1902E-11	1.4332E-11	1.6909E-11	1.9929E-11	2.4004E-11
51	73.7130	2.9147E-12	3.8844E-12	4.8408E-12	5.9456E-12	7.2790E-12	8.8710E-12	1.0701E-11	1.2685E-11	1.4999E-11	1.8069E-11
52	75.2130	2.0842E-12	2.7831E-12	3.4727E-12	4.2729E-12	5.2362E-12	6.3935E-12	7.7381E-12	9.2290E-12	1.0967E-11	1.3246E-11

POINT	GROUP / RADIUS	11	12	13	14	15	16	17	18	19	20
1	0.0	0.0	0.0	0.0	0.0	0.0	0.0	0.0	0.0	0.0	0.0
2	1.5071	5.0495E-10	7.5829E-10	8.5935E-10	9.7325E-10	9.2860E-10	9.7748E-10	1.2570E-09	1.4157E-09	1.5342E-09	1.6158E-09

3	3.0142	1.0082E-09	1.5141E-09	1.7158E-09	1.9432E-09	1.8541E-09	1.9517E-09	2.5097E-09	2.8266E-09	3.0632E-09	3.2262E-09
4	4.5213	1.5082E-09	2.2650E-09	2.5667E-09	2.9069E-09	2.7734E-09	2.9194E-09	3.7542E-09	4.2283E-09	4.5823E-09	4.8260E-09
5	6.0284	2.0033E-09	3.0086E-09	3.4093E-09	3.8611E-09	3.6837E-09	3.8775E-09	4.9865E-09	5.6162E-09	6.0864E-09	6.4101E-09
6	7.5355	2.4920E-09	3.7426E-09	4.2409E-09	4.8027E-09	4.5820E-09	4.8230E-09	6.2027E-09	6.9860E-09	7.5709E-09	7.9733E-09
7	9.0426	2.9727E-09	4.4648E-09	5.0589E-09	5.7290E-09	5.4654E-09	5.7529E-09	7.3989E-09	8.3334E-09	9.0311E-09	9.5108E-09
8	10.5497	3.4441E-09	5.1729E-09	5.8609E-09	6.6370E-09	6.3314E-09	6.6644E-09	8.5717E-09	9.6544E-09	1.0463E-08	1.1018E-08
9	12.0568	3.9048E-09	5.8651E-09	6.6445E-09	7.5241E-09	7.1774E-09	7.5548E-09	9.7176E-09	1.0945E-08	1.1861E-08	1.2491E-08
10	13.5639	4.3536E-09	6.5393E-09	7.4076E-09	8.3878E-09	8.0011E-09	8.4218E-09	1.0833E-08	1.2202E-08	1.3223E-08	1.3924E-08
11	15.0710	4.7895E-09	7.1939E-09	8.1481E-09	9.2259E-09	8.8002E-09	9.2630E-09	1.1916E-08	1.3422E-08	1.4545E-08	1.5316E-08
12	16.5781	5.2115E-09	7.8273E-09	8.8643E-09	1.0036E-08	9.5731E-09	1.0077E-08	1.2964E-08	1.4602E-08	1.5824E-08	1.6661E-08
13	18.0852	5.6188E-09	8.4383E-09	9.5545E-09	1.0817E-08	1.0318E-08	1.0861E-08	1.3974E-08	1.5740E-08	1.7058E-08	1.7959E-08
14	19.5923	6.0109E-09	9.0255E-09	1.0217E-08	1.1567E-08	1.1034E-08	1.1615E-08	1.4944E-08	1.6833E-08	1.8243E-08	1.9205E-08
15	21.0994	6.3873E-09	9.5882E-09	1.0852E-08	1.2284E-08	1.1719E-08	1.2337E-08	1.5874E-08	1.7880E-08	1.9378E-08	2.0400E-08
16	22.6065	6.7479E-09	1.0126E-08	1.1457E-08	1.2968E-08	1.2373E-08	1.3028E-08	1.6762E-08	1.8881E-08	2.0464E-08	2.1541E-08
17	24.1136	7.0929E-09	1.0638E-08	1.2033E-08	1.3618E-08	1.2997E-08	1.3686E-08	1.7608E-08	1.9834E-08	2.1498E-08	2.2628E-08
18	25.6207	7.4225E-09	1.1124E-08	1.2578E-08	1.4233E-08	1.3589E-08	1.4313E-08	1.8413E-08	2.0740E-08	2.2481E-08	2.3661E-08
19	27.1278	7.7376E-09	1.1584E-08	1.3094E-08	1.4815E-08	1.4151E-08	1.4909E-08	1.9176E-08	2.1599E-08	2.3415E-08	2.4643E-08
20	28.6349	8.0392E-09	1.2020E-08	1.3580E-08	1.5362E-08	1.4684E-08	1.5476E-08	1.9899E-08	2.2414E-08	2.4301E-08	2.5574E-08
21	30.1420	8.3287E-09	1.2431E-08	1.4037E-08	1.5877E-08	1.5190E-08	1.6017E-08	2.0584E-08	2.3186E-08	2.5141E-08	2.6458E-08
22	31.6491	8.6081E-09	1.2819E-08	1.4466E-08	1.6359E-08	1.5670E-08	1.6534E-08	2.1234E-08	2.3918E-08	2.5941E-08	2.7299E-08
23	33.1562	8.8798E-09	1.3186E-08	1.4870E-08	1.6812E-08	1.6129E-08	1.7032E-08	2.1853E-08	2.4615E-08	2.6704E-08	2.8102E-08
24	34.6633	9.1470E-09	1.3532E-08	1.5249E-08	1.7237E-08	1.6570E-08	1.7515E-08	2.2445E-08	2.5281E-08	2.7437E-08	2.8875E-08
25	36.1704	9.4132E-09	1.3861E-08	1.5605E-08	1.7636E-08	1.6998E-08	1.7991E-08	2.3016E-08	2.5924E-08	2.8147E-08	2.9625E-08
26	37.6775	9.6831E-09	1.4174E-08	1.5943E-08	1.8013E-08	1.7419E-08	1.8467E-08	2.3571E-08	2.6550E-08	2.8843E-08	3.0364E-08
27	39.1846	9.9623E-09	1.4475E-08	1.6264E-08	1.8371E-08	1.7840E-08	1.8953E-08	2.4120E-08	2.7168E-08	2.9536E-08	3.1103E-08
28	40.6917	1.0257E-08	1.4766E-08	1.6573E-08	1.8715E-08	1.8270E-08	1.9461E-08	2.4670E-08	2.7789E-08	3.0240E-08	3.1857E-08
29	42.1988	1.0576E-08	1.5052E-08	1.6874E-08	1.9050E-08	1.8720E-08	2.0003E-08	2.5232E-08	2.8425E-08	3.0968E-08	3.2642E-08
30	43.7059	1.0928E-08	1.5335E-08	1.7170E-08	1.9380E-08	1.9202E-08	2.0599E-08	2.5819E-08	2.9091E-08	3.1741E-08	3.3482E-08
31	45.2130	1.1324E-08	1.5620E-08	1.7468E-08	1.9711E-08	1.9731E-08	2.1269E-08	2.6445E-08	2.9804E-08	3.2579E-08	3.4400E-08
32	45.2130	1.1324E-08	1.5620E-08	1.7468E-08	1.9711E-08	1.9731E-08	2.1269E-08	2.6445E-08	2.9804E-08	3.2579E-08	3.4400E-08
33	46.7130	7.9099E-09	1.0871E-08	1.2326E-08	1.3993E-08	1.4201E-08	1.5326E-08	1.8818E-08	2.1160E-08	2.3088E-08	2.4403E-08
34	48.2130	5.5224E-09	7.5643E-09	8.6880E-09	9.9188E-09	1.0194E-08	1.1014E-08	1.3371E-08	1.5001E-08	1.6341E-08	1.7285E-08
35	49.7130	3.8597E-09	5.2708E-09	6.1256E-09	7.0312E-09	7.3093E-09	7.9064E-09	9.5015E-09	1.0636E-08	1.1567E-08	1.2244E-08
36	51.2130	2.7016E-09	3.6787E-09	4.3220E-09	4.9864E-09	5.2379E-09	5.6723E-09	6.7545E-09	7.5451E-09	8.1930E-09	8.6772E-09
37	52.7130	1.8944E-09	2.5726E-09	3.0528E-09	3.5392E-09	3.7535E-09	4.0694E-09	4.8057E-09	5.3571E-09	5.8088E-09	6.1550E-09
38	54.2130	1.3315E-09	1.8032E-09	2.1596E-09	2.5151E-09	2.6911E-09	2.9211E-09	3.4236E-09	3.8088E-09	4.1244E-09	4.3720E-09
39	55.7130	9.3840E-10	1.2675E-09	1.5307E-09	1.7904E-09	1.9315E-09	2.0991E-09	2.4433E-09	2.7129E-09	2.9340E-09	3.1114E-09
40	57.2130	6.6356E-10	8.9378E-10	1.0877E-09	1.2773E-09	1.3886E-09	1.5110E-09	1.7477E-09	1.9369E-09	2.0923E-09	2.2197E-09
41	58.7130	4.7108E-10	6.3268E-10	7.7524E-10	9.1385E-10	1.0006E-09	1.0902E-09	1.2537E-09	1.3869E-09	1.4967E-09	1.5884E-09
42	60.2130	3.3600E-10	4.4987E-10	5.5461E-10	6.5604E-10	7.2314E-10	7.8895E-10	9.0247E-10	9.9673E-10	1.0746E-09	1.1409E-09
43	61.7130	2.4097E-10	3.2155E-10	3.9855E-10	4.7291E-10	5.2459E-10	5.7314E-10	6.5243E-10	7.1943E-10	7.7503E-10	8.2327E-10
44	63.2130	1.7392E-10	2.3124E-10	2.8792E-10	3.4260E-10	3.8229E-10	4.1829E-10	4.7406E-10	5.2198E-10	5.6197E-10	5.9728E-10
45	64.7130	1.2645E-10	1.6745E-10	2.0928E-10	2.4964E-10	2.8012E-10	3.0699E-10	3.4652E-10	3.8104E-10	4.1005E-10	4.3611E-10
46	66.2130	9.2698E-11	1.2223E-10	1.5321E-10	1.8314E-10	2.0657E-10	2.2677E-10	2.5506E-10	2.8014E-10	3.0139E-10	3.2081E-10
47	67.7130	6.8571E-11	8.9996E-11	1.1305E-10	1.3537E-10	1.5345E-10	1.6875E-10	1.8921E-10	2.0762E-10	2.2337E-10	2.3799E-10
48	69.2130	5.1195E-11	6.6865E-11	8.4121E-11	1.0087E-10	1.1488E-10	1.2659E-10	1.4156E-10	1.5523E-10	1.6705E-10	1.7819E-10
49	70.7130	3.8538E-11	5.0094E-11	6.3089E-11	7.5755E-11	8.6673E-11	9.5720E-11	1.0681E-10	1.1709E-10	1.2608E-10	1.3469E-10
50	72.2130	2.9149E-11	3.7731E-11	4.7577E-11	5.7222E-11	6.5781E-11	7.2840E-11	8.1163E-11	8.8982E-11	9.5921E-11	1.0266E-10
51	73.7130	2.1962E-11	2.8358E-11	3.5852E-11	4.3239E-11	4.9980E-11	5.5530E-11	6.1839E-11	6.7849E-11	7.3267E-11	7.8592E-11
52	75.2130	1.6161E-11	2.0908E-11	2.6612E-11	3.2280E-11	3.7593E-11	4.1964E-11	4.6763E-11	5.1399E-11	5.5655E-11	5.9882E-11

	GROUP	21	22	23	24	25	26	27	28	29	30
POINT	RADIUS										
1	0.0	0.0	0.0	0.0	0.0	0.0	0.0	0.0	0.0	0.0	0.0
2	1.5071	2.0091E-09	2.2126E-09	2.3008E-09	2.3681E-09	2.3878E-09	2.2228E-09	2.3709E-09	2.4902E-09	2.3792E-09	2.3758E-09
3	3.0142	4.0114E-09	4.4178E-09	4.5939E-09	4.7283E-09	4.7676E-09	4.4381E-09	4.7337E-09	4.9719E-09	4.7505E-09	4.7436E-09
4	4.5213	6.0007E-09	6.6086E-09	6.8720E-09	7.0730E-09	7.1319E-09	6.6387E-09	7.0811E-09	7.4374E-09	7.1061E-09	7.0957E-09
5	6.0284	7.9704E-09	8.7779E-09	9.1276E-09	9.3947E-09	9.4728E-09	8.8176E-09	9.4052E-09	9.8786E-09	9.4386E-09	9.4246E-09
6	7.5355	9.9144E-09	1.0919E-08	1.1354E-08	1.1686E-08	1.1783E-08	1.0968E-08	1.1699E-08	1.2288E-08	1.1740E-08	1.1723E-08
7	9.0426	1.1826E-08	1.3025E-08	1.3543E-08	1.3940E-08	1.4056E-08	1.3082E-08	1.3955E-08	1.4658E-08	1.4005E-08	1.3983E-08
8	10.5497	1.3701E-08	1.5089E-08	1.5690E-08	1.6149E-08	1.6283E-08	1.5155E-08	1.6167E-08	1.6981E-08	1.6224E-08	1.6199E-08
9	12.0568	1.5532E-08	1.7106E-08	1.7787E-08	1.8308E-08	1.8460E-08	1.7180E-08	1.8328E-08	1.9252E-08	1.8393E-08	1.8364E-08
10	13.5639	1.7316E-08	1.9070E-08	1.9829E-08	2.0410E-08	2.0580E-08	1.9152E-08	2.0432E-08	2.1464E-08	2.0506E-08	2.0473E-08
11	15.0710	1.9046E-08	2.0976E-08	2.1811E-08	2.2450E-08	2.2637E-08	2.1066E-08	2.2476E-08	2.3611E-08	2.2558E-08	2.2521E-08
12	16.5781	2.0720E-08	2.2819E-08	2.3728E-08	2.4424E-08	2.4628E-08	2.2917E-08	2.4453E-08	2.5691E-08	2.4544E-08	2.4503E-08
13	18.0852	2.2333E-08	2.4595E-08	2.5575E-08	2.6327E-08	2.6548E-08	2.4703E-08	2.6361E-08	2.7698E-08	2.6461E-08	2.6416E-08

etc

DETAILED NEUTRON BALANCES FOR EACH ZONE

LEAKAGE COMPONENTS FOR ZONE 1

GROUP	LEFT EDGE J OUT	LEFT EDGE J IN	LEFT EDGE NET J	RIGHT EDGE J OUT	RIGHT EDGE J IN	RIGHT EDGE NET J	BUCKLING LEAKAGE	TOTAL LEAKAGE
1	0.0	0.0	0.0	3.9206E-05	-2.9681E-06	4.2174E-05	0.0	4.2174E-05
2	0.0	0.0	0.0	5.2770E-05	-3.7980E-06	5.6568E-05	0.0	5.6568E-05
3	0.0	0.0	0.0	6.6487E-05	-4.6909E-06	7.1178E-05	0.0	7.1178E-05
4	0.0	0.0	0.0	8.1872E-05	-5.5569E-06	8.7429E-05	0.0	8.7429E-05
5	0.0	0.0	0.0	1.0437E-04	-7.2350E-06	1.1161E-04	0.0	1.1161E-04
6	0.0	0.0	0.0	1.2920E-04	-8.6211E-06	1.3782E-04	0.0	1.3782E-04
7	0.0	0.0	0.0	1.5353E-04	-9.1711E-06	1.6270E-04	0.0	1.6270E-04
8	0.0	0.0	0.0	1.6269E-04	-6.4925E-06	1.6918E-04	0.0	1.6918E-04
9	0.0	0.0	0.0	1.8449E-04	-5.2752E-06	1.8976E-04	0.0	1.8976E-04
10	0.0	0.0	0.0	2.3377E-04	-6.7931E-06	2.4056E-04	0.0	2.4056E-04
11	0.0	0.0	0.0	2.8503E-04	-5.8678E-06	2.9090E-04	0.0	2.9090E-04
12	0.0	0.0	0.0	3.9389E-04	-7.3563E-06	4.0124E-04	0.0	4.0124E-04
13	0.0	0.0	0.0	4.5128E-04	2.5544E-06	4.4873E-04	0.0	4.4873E-04
14	0.0	0.0	0.0	5.1697E-04	1.0617E-05	5.0635E-04	0.0	5.0635E-04
15	0.0	0.0	0.0	5.3067E-04	2.3820E-05	5.0685E-04	0.0	5.0685E-04
16	0.0	0.0	0.0	5.7735E-04	3.0996E-05	5.4635E-04	0.0	5.4635E-04
17	0.0	0.0	0.0	7.1121E-04	3.1884E-05	6.7933E-04	0.0	6.7933E-04
18	0.0	0.0	0.0	8.0411E-04	3.8493E-05	7.6562E-04	0.0	7.6562E-04
19	0.0	0.0	0.0	8.8310E-04	4.6208E-05	8.3689E-04	0.0	8.3689E-04
20	0.0	0.0	0.0	9.3938E-04	5.5695E-05	8.8369E-04	0.0	8.8369E-04
21	0.0	0.0	0.0	1.1169E-03	5.6770E-05	1.0601E-03	0.0	1.0601E-03
22	0.0	0.0	0.0	1.2340E-03	6.5714E-05	1.1683E-03	0.0	1.1683E-03
23	0.0	0.0	0.0	1.3054E-03	7.4149E-05	1.2312E-03	0.0	1.2312E-03
24	0.0	0.0	0.0	1.3765E-03	8.2865E-05	1.2936E-03	0.0	1.2936E-03
25	0.0	0.0	0.0	1.4348E-03	9.4796E-05	1.3400E-03	0.0	1.3400E-03
26	0.0	0.0	0.0	1.4175E-03	1.0948E-04	1.3080E-03	0.0	1.3080E-03
27	0.0	0.0	0.0	1.5419E-03	1.1331E-04	1.4286E-03	0.0	1.4286E-03
28	0.0	0.0	0.0	1.6534E-03	1.2047E-04	1.5329E-03	0.0	1.5329E-03
29	0.0	0.0	0.0	1.6078E-03	1.2913E-04	1.4787E-03	0.0	1.4787E-03
30	0.0	0.0	0.0	1.6359E-03	1.4162E-04	1.4942E-03	0.0	1.4942E-03
31	0.0	0.0	0.0	1.6025E-03	1.5517E-04	1.4473E-03	0.0	1.4473E-03
32	0.0	0.0	0.0	1.6943E-03	1.5998E-04	1.5344E-03	0.0	1.5344E-03
33	0.0	0.0	0.0	1.8574E-03	1.6774E-04	1.6896E-03	0.0	1.6896E-03
34	0.0	0.0	0.0	2.0094E-03	1.7689E-04	1.8325E-03	0.0	1.8325E-03
35	0.0	0.0	0.0	2.2775E-03	1.7828E-04	2.0992E-03	0.0	2.0992E-03
36	0.0	0.0	0.0	2.6613E-03	1.7565E-04	2.4856E-03	0.0	2.4856E-03
37	0.0	0.0	0.0	2.7270E-03	1.9992E-04	2.5271E-03	0.0	2.5271E-03
38	0.0	0.0	0.0	2.2559E-03	2.5321E-04	2.0027E-03	0.0	2.0027E-03
39	0.0	0.0	0.0	2.7022E-03	2.3596E-04	2.4662E-03	0.0	2.4662E-03
40	0.0	0.0	0.0	2.9324E-03	2.5739E-04	2.6750E-03	0.0	2.6750E-03
41	0.0	0.0	0.0	3.2172E-03	2.7666E-04	2.9405E-03	0.0	2.9405E-03
42	0.0	0.0	0.0	3.2648E-03	3.0722E-04	2.9576E-03	0.0	2.9576E-03
43	0.0	0.0	0.0	4.0554E-03	3.8799E-04	3.6675E-03	0.0	3.6675E-03
44	0.0	0.0	0.0	4.2781E-03	4.0826E-04	3.8698E-03	0.0	3.8698E-03
45	0.0	0.0	0.0	4.4520E-03	4.2678E-04	4.0253E-03	0.0	4.0253E-03
46	0.0	0.0	0.0	4.3242E-03	4.3449E-04	3.8898E-03	0.0	3.8898E-03
47	0.0	0.0	0.0	3.8551E-03	4.6214E-04	3.3930E-03	0.0	3.3930E-03
48	0.0	0.0	0.0	4.5100E-03	4.2235E-04	4.0877E-03	0.0	4.0877E-03
49	0.0	0.0	0.0	4.5687E-03	4.0683E-04	4.1619E-03	0.0	4.1619E-03
50	0.0	0.0	0.0	4.5837E-03	3.7703E-04	4.2066E-03	0.0	4.2066E-03
51	0.0	0.0	0.0	4.5823E-03	3.4341E-04	4.2389E-03	0.0	4.2389E-03
52	0.0	0.0	0.0	4.8059E-03	3.1261E-04	4.4933E-03	0.0	4.4933E-03
53	0.0	0.0	0.0	4.5568E-03	3.4147E-04	4.2153E-03	0.0	4.2153E-03
54	0.0	0.0	0.0	4.8518E-03	3.6022E-04	4.4916E-03	0.0	4.4916E-03
55	0.0	0.0	0.0	4.7942E-03	4.2920E-04	4.3650E-03	0.0	4.3650E-03

etc.

188	0.0	0.0	0.0	1.0744E-03	6.2168E-04	4.5272E-04	0.0	4.5272E-04
189	0.0	0.0	0.0	1.0643E-03	6.1985E-04	4.4441E-04	0.0	4.4441E-04
190	0.0	0.0	0.0	1.0227E-03	6.0941E-04	4.1326E-04	0.0	4.1326E-04
191	0.0	0.0	0.0	9.9466E-04	5.9548E-04	3.9918E-04	0.0	3.9918E-04
192	0.0	0.0	0.0	9.3737E-04	5.7480E-04	3.6258E-04	0.0	3.6258E-04
193	0.0	0.0	0.0	8.8037E-04	5.4512E-04	3.3525E-04	0.0	3.3525E-04
194	0.0	0.0	0.0	7.3515E-04	4.4985E-04	2.8529E-04	0.0	2.8529E-04
195	0.0	0.0	0.0	7.5376E-04	4.4393E-04	3.0983E-04	0.0	3.0983E-04
196	0.0	0.0	0.0	7.1604E-04	4.3648E-04	2.7957E-04	0.0	2.7957E-04
197	0.0	0.0	0.0	5.9019E-03	3.6260E-03	2.2759E-03	0.0	2.2759E-03
198	0.0	0.0	0.0	2.1243E-03	1.2765E-03	8.4781E-04	0.0	8.4781E-04
199	0.0	0.0	0.0	6.4256E-04	3.4189E-04	3.0067E-04	0.0	3.0067E-04
200	0.0	0.0	0.0	1.0476E-04	5.8997E-05	4.5767E-05	0.0	4.5767E-05
201	0.0	0.0	0.0	2.2502E-05	7.6903E-06	1.4811E-05	0.0	1.4811E-05
202	0.0	0.0	0.0	2.4245E-06	1.0150E-06	1.4095E-06	0.0	1.4095E-06
203	0.0	0.0	0.0	3.2112E-07	5.4176E-08	2.6694E-07	0.0	2.6694E-07
204	0.0	0.0	0.0	1.4943E-07	6.8596E-08	8.0832E-08	0.0	8.0832E-08
205	0.0	0.0	0.0	1.6289E-08	1.2107E-08	4.1823E-09	0.0	4.1823E-09
206	0.0	0.0	0.0	1.3049E-09	1.2358E-09	6.9123E-11	0.0	6.9123E-11
207	0.0	0.0	0.0	6.9958E-12	4.8340E-11	-4.1344E-11	0.0	-4.1344E-11
208	0.0	0.0	0.0	1.7918E-13	1.2922E-12	-1.1130E-12	0.0	-1.1130E-12
SUM OVER GROUPS	0.0	0.0	0.0	1.0297D+00	6.5750D-01	3.7222D-01	0.0	3.7222D-01

BALANCE EQUATION FOR ZONE 1

GROUP	TOTAL LEAKAGE	+ CAPTURE RATE	+ FISSION REMOVAL	+ OUT SCATTER	- IN SCATTER	- FISSION PRODUCTION	- EXTERNAL SOURCE	= BALANCE	, COLLISION RATE
1	4.2174E-05	2.0884E-05	2.9595E-05	1.7507E-04	0.0	2.9357E-04	0.0	-2.5842E-05	3.2470E-04
2	5.6568E-05	2.0116E-05	3.9868E-05	2.4516E-04	2.2739E-05	3.7169E-04	0.0	-3.2719E-05	4.4269E-04
3	7.1178E-05	2.1276E-05	5.0500E-05	3.2128E-04	3.9478E-05	4.6575E-04	0.0	-4.0999E-05	5.7399E-04
4	8.7429E-05	2.2012E-05	6.2710E-05	4.1022E-04	5.5433E-05	5.7780E-04	0.0	-5.0863E-05	7.2473E-04
5	1.1161E-04	2.3835E-05	7.9654E-05	5.0587E-04	7.3549E-05	7.0991E-04	0.0	-6.2492E-05	9.0448E-04
6	1.3782E-04	2.5731E-05	9.8437E-05	6.1828E-04	9.2130E-05	8.6421E-04	0.0	-7.6074E-05	1.1148E-03
7	1.6270E-04	2.9836E-05	1.1809E-04	7.5559E-04	1.1542E-04	1.0426E-03	0.0	-9.1774E-05	1.3695E-03
8	1.6918E-04	3.8321E-05	1.2987E-04	9.4398E-04	1.4420E-04	1.2469E-03	0.0	-1.0976E-04	1.6555E-03
9	1.8976E-04	3.9589E-05	1.4879E-04	1.1623E-03	1.9173E-04	1.4789E-03	0.0	-1.3019E-04	2.0321E-03
10	2.4056E-04	4.0345E-05	1.8426E-04	1.3857E-03	2.6401E-04	1.7400E-03	0.0	-1.5317E-04	2.4780E-03
11	2.9090E-04	4.1555E-05	2.2098E-04	1.6335E-03	3.3425E-04	2.0315E-03	0.0	-1.7882E-04	2.9963E-03
12	4.0124E-04	4.8687E-05	2.8707E-04	1.8179E-03	4.0809E-04	2.3540E-03	0.0	-2.0722E-04	3.6274E-03
13	4.4873E-04	4.9408E-05	3.1933E-04	2.0943E-03	4.4201E-04	2.7082E-03	0.0	-2.3840E-04	4.2616E-03
14	5.0635E-04	5.2768E-05	3.4964E-04	2.4254E-03	5.1247E-04	3.0941E-03	0.0	-2.7236E-04	4.9710E-03
15	5.0685E-04	5.4319E-05	3.4361E-04	2.9313E-03	5.9441E-04	3.5546E-03	0.0	-3.1290E-04	5.7419E-03
16	5.4635E-04	5.3630E-05	3.4529E-04	3.4346E-03	7.1952E-04	4.0137E-03	0.0	-3.5331E-04	6.6230E-03
17	6.7933E-04	6.0680E-05	3.9130E-04	3.8786E-03	9.0311E-04	4.5032E-03	0.0	-3.9641E-04	7.6744E-03
18	7.6562E-04	6.4625E-05	4.3146E-04	4.4143E-03	1.0964E-03	5.0216E-03	0.0	-4.4204E-04	8.7379E-03
19	8.3689E-04	6.5695E-05	4.7084E-04	4.9865E-03	1.2834E-03	5.5666E-03	0.0	-4.9001E-04	9.9178E-03
20	8.8369E-04	6.5915E-05	5.0079E-04	5.6218E-03	1.4766E-03	6.1357E-03	0.0	-5.4011E-04	1.0941E-02
21	1.0601E-03	7.0663E-05	5.8068E-04	6.1666E-03	1.7442E-03	6.7259E-03	0.0	-5.9207E-04	1.2484E-02
22	1.1683E-03	7.4773E-05	6.4354E-04	6.8702E-03	2.0682E-03	7.3342E-03	0.0	-6.4562E-04	1.3936E-02
23	1.2312E-03	7.6582E-05	6.8640E-04	7.6763E-03	2.4141E-03	7.9568E-03	0.0	-7.0042E-04	1.5122E-02
24	1.2936E-03	7.8987E-05	7.3406E-04	8.5581E-03	2.8309E-03	8.5900E-03	0.0	-7.5615E-04	1.6435E-02
25	1.3400E-03	8.1034E-05	7.8141E-04	9.5320E-03	3.3170E-03	9.2299E-03	0.0	-8.1248E-04	1.7794E-02
26	1.3080E-03	7.9126E-05	7.9856E-04	1.0606E-02	3.7885E-03	9.8725E-03	0.0	-8.6905E-04	1.9226E-02
27	1.4286E-03	8.3596E-05	8.8458E-04	1.1633E-02	4.4413E-03	1.0514E-02	0.0	-9.2549E-04	2.1278E-02
28	1.5329E-03	8.7055E-05	9.6721E-04	1.2718E-02	5.1377E-03	1.1149E-02	0.0	-9.8145E-04	2.2966E-02
29	1.4787E-03	8.1925E-05	9.5523E-04	1.2901E-02	5.3005E-03	1.1093E-02	0.0	-9.7648E-04	2.3111E-02
30	1.4942E-03	8.1909E-05	9.8427E-04	1.3728E-02	5.6614E-03	1.1653E-02	0.0	-1.0258E-03	2.4005E-02
31	1.4473E-03	6.8772E-05	9.7915E-04	1.4636E-02	6.0070E-03	1.2198E-02	0.0	-1.0737E-03	2.4617E-02
32	1.5344E-03	6.3791E-05	1.0369E-03	1.5510E-02	6.5407E-03	1.2724E-02	0.0	-1.1201E-03	2.6319E-02
33	1.6896E-03	8.0414E-05	1.1415E-03	1.6603E-02	7.4488E-03	1.3230E-02	0.0	-1.1646E-03	2.8616E-02
34	1.8325E-03	8.5195E-05	1.2427E-03	1.7706E-02	8.3608E-03	1.3713E-02	0.0	-1.2071E-03	3.0471E-02

etc.

190	-4.0495E-04	3.7507E-04	1.6161E-05	2.1737E-03	2.1599E-03	0.0	0.0	-6.9849E-10	1.0481E-02
191	-3.9030E-04	3.7424E-04	1.6092E-05	2.1767E-03	2.1767E-03	0.0	0.0	-4.6566E-10	1.0459E-02
192	-3.5319E-04	3.7056E-04	1.4914E-05	2.1474E-03	2.1797E-03	0.0	0.0	-1.1642E-09	1.0288E-02
193	-3.2558E-04	3.8480E-04	1.7371E-05	2.0743E-03	2.1509E-03	0.0	0.0	-4.6566E-10	9.9787E-03
194	-2.7731E-04	5.8967E-04	1.3307E-05	1.7527E-03	2.0784E-03	0.0	0.0	-6.9849E-10	8.5865E-03
195	-3.0150E-04	3.2244E-04	1.3816E-05	1.7275E-03	1.7623E-03	0.0	0.0	-9.3132E-10	8.2009E-03
196	-2.7103E-04	2.8638E-04	1.0157E-05	1.7045E-03	1.7300E-03	0.0	0.0	-6.9849E-10	8.0490E-03
197	-2.2019E-03	3.1507E-03	1.3605E-04	6.7474E-04	1.7595E-03	0.0	0.0	-2.7940E-09	7.2628E-02
198	-8.2049E-04	1.0811E-03	7.0877E-05	3.4510E-04	6.7659E-04	0.0	0.0	0.0	2.8823E-02
199	-2.9139E-04	5.6050E-04	2.5254E-05	5.0848E-05	3.4521E-04	0.0	0.0	2.3283E-10	7.3600E-03
200	-4.4628E-05	8.0562E-05	5.7895E-06	9.1478E-06	5.0872E-05	0.0	0.0	0.0	1.0911E-03
201	-1.4745E-05	2.2108E-05	8.4805E-07	9.4186E-07	9.1529E-06	0.0	0.0	-5.4570E-12	1.4751E-04
202	-1.4070E-06	2.1784E-06	9.6954E-08	7.4663E-08	9.4295E-07	0.0	0.0	-5.6843E-13	1.1295E-05
203	-2.6690E-07	3.2589E-07	6.8741E-09	9.0330E-09	7.4900E-08	0.0	0.0	-5.6843E-14	1.0734E-06
204	-8.0284E-08	7.2642E-08	3.5224E-09	1.3204E-08	9.0840E-09	0.0	0.0	6.3949E-14	9.4676E-07
205	-3.8434E-09	1.2877E-08	1.4687E-09	2.7119E-09	1.3215E-08	0.0	0.0	0.0	2.1821E-07
206	6.8624E-12	2.0421E-09	3.7570E-10	2.8963E-10	2.7143E-09	0.0	0.0	-6.6613E-16	2.9895E-08
207	4.7852E-11	1.7139E-10	5.4093E-11	1.6801E-11	2.9014E-10	0.0	0.0	-2.2204E-16	1.8593E-09
208	1.3901E-12	1.2151E-11	3.3990E-12	-1.1323E-19	1.6940E-11	0.0	0.0	0.0	7.7759E-11
SUM OVER GROUPS	-3.2582D-01	3.8602D-01	3.2017D-02	4.2055D+00	4.2049D+00	1.0544D+00	0.0	-9.6158D-01	1.7948D+01

NORMAL END OF MANDI CALCULATION